

Optimal Virtual Tube Planning and Control for Swarm Robotics

Journal Title
XX(X):1-18
©The Author(s) 2022
Reprints and permission:
sagepub.co.uk/journalsPermissions.nav
DOI: 10.1177/ToBeAssigned
www.sagepub.com/

SAGE

Pengda Mao¹ and Quan Quan¹

Abstract

This paper presents a novel method for efficiently solving trajectory planning problems for swarm robotics in cluttered environments. While recent research has demonstrated high success rates in real-time local trajectory planning for swarm robotics in cluttered environments, optimizing every trajectory for each robot is computationally expensive, with a computational complexity of $O(n^2)$ to $O(n^3)$. To address this issue, we first propose the concept of the *optimal virtual tube*, which includes infinite optimal trajectories. Under certain conditions, any optimal trajectory in the optimal virtual tube can be expressed as a convex combination of a finite number of optimal trajectories, with a computational complexity of $O(1)$. Afterward, a planning method of *the optimal virtual tube* is proposed. In simulations and experiments, we show that the proposed method efficiently reduces calculation and is validated by comparison with traditional methods.

Keywords

Swarm robotics, Trajectory planning, Virtual tube, Optimization

Introduction

Swarm robotics has potential applications in various real-world scenarios, such as air traffic control, land and sea search and rescue, and target detection. Therefore, it is important to enable swarm robotics to navigate through environments with dense obstacles smoothly and safely.

Trajectory planning is an efficient method for robots to pass through a complex environment. By leveraging the differential flatness of the drone, a smooth and safe trajectory is planned and tracked by the drone. The trajectory can be parameterized as a k -th order polynomials (Mellinger and Kumar (2011)), which can pass through fixed waypoints. However, polynomials are susceptible to collisions with obstacles due to the finite discrete avoidance constraints. To address this issue, various methods have been proposed for generating collision-free trajectories. For instance, a collision-free trajectory has been generated early with mixed integer methods in Deits and Tedrake (2015). The approach proposed by Richter et al. (2016) refines the trajectory iteratively by minimizing a cost function and adding additional waypoints between two ends of a particular trajectory segment that passes through obstacles to avoid collisions. However, these methods can be computationally intensive and may not be suitable for real-time planning. To overcome these challenges, some methods have been proposed that use simple constraints to design a QP problem, which can significantly reduce computation time. For example, a safe flight corridor (SFC), which is a collection of convex connected polyhedra that models free space in a map, is used as a constraint for obstacle avoidance to generate a collision-free trajectory in real time (Liu et al. (2017); Gao et al. (2020)). The trajectory parameterized by B-spline (Usenko et al. (2017)) is proposed to eliminate constraints of intermediate conditions on any

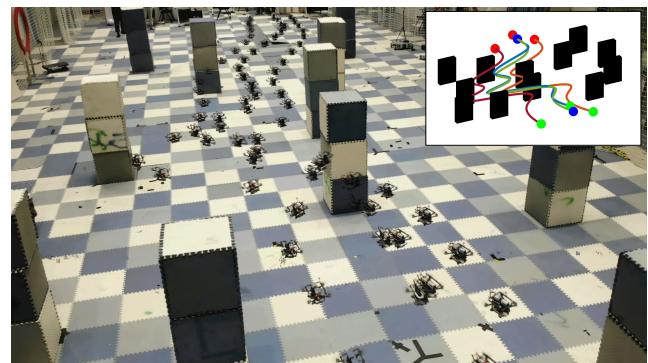


Figure 1. Optimal virtual tube method: An overlay image of four drones passing through the cluttered environment. The trajectory of each drone is represented by a different colored line in the upper right figure. Compared to the traditional method, our method solves only three optimization problems for the three optimal trajectories of drones, such as the red, blue, and orange lines. The fourth optimal trajectory of the drone (the green line) is generated by an affine combination.

derivative of the trajectory. An essential advantage of using B-splines is their convex hull property, which bounds both the trajectory and its derivatives. This property allows for strict bounding of the position, velocity, and acceleration of a robot (Ding et al. (2019)). The drawback of the B-spline, however, is that the B-spline curve does not pass through the control points that represent waypoints. To repel

¹ School of Automation Science and Electrical Engineering, Beihang University, Beijing, P.R. China

Corresponding author:

Quan Quan, School of Automation Science and Electrical Engineering, Beihang University, Beijing, 100191, P.R. China.

Email: qq.buaa@buaa.edu.cn

the trajectory from obstacles, a gradient-based method is applied (Zhou et al. (2020, 2021a)) as a penalty. Although this method has been successful, it depends on experience and lacks strict theoretical proof. It has been shown that if the control points satisfy conditions, the trajectory will strictly avoid obstacles (Zhou et al. (2019)). To plan swarm trajectories, existing methods are typically extended from single trajectory planning methods. However, in swarm robotics, other agents are regarded as dynamic obstacles, which adds to the complexity of trajectory planning. Several methods have been proposed to solve this avoidance problem, such as SFC (Park and Kim (2021)), distributed model predictive control (Soria et al. (2022)), HOOP (Tang et al. (2018)) and EGO-Swarm (Zhou et al. (2021b)), all of which employ increasingly complex constraints. All safe and smooth trajectories need to be generated by optimization problems, which require significant computational resources with an increasing scale of the swarm. Therefore, the efficiency of the methods for swarm robotics is a crucial point needed to be considered, especially given the limited onboard computing resources of robots.

The objective of trajectory planning in passing through an environment is to plan a trajectory from a start position to a goal position for each robot. Ideally, trajectory planning would yield a unique solution to the optimization problem, but Orthey et al. (2019) demonstrates that local minima in the optimization problem result in an infinite set of homotopic collision-free trajectories. To address this challenge, a generative model of collision-free trajectory is trained in Osa (2022) to represent an infinite set of homotopic solutions to the optimization problem. Motivated by the methods for finding homotopic trajectories for a robot, we proposed an *optimal virtual tube* for swarm robotics, which contains an infinite number of homotopic optimal trajectories in free space. Our focus is on finding infinite trajectories for a swarm, rather than for a single robot, although generating infinite optimal trajectories through infinite optimization problems is not feasible due to computational complexity. To mitigate this issue, we first propose and define the optimal virtual tube, including infinite optimal trajectories. Under certain conditions, any optimal trajectory in the optimal virtual tube is a convex combination of a finite number of optimal trajectories, with a computational complexity of $O(1)$. Therefore, combining the advantages of formation control (Alonso-Mora et al. (2017)), the complexity of the optimal virtual tube planning is independent of the scale of the swarm.

A *virtual tube*, defined in previous studies (Quan et al. (2022); Mao and Quan (2022); Gao et al. (2022); Quan et al. (2023b)), is a space for the swarm robotics flow. There are two problems summarized, namely the *virtual tube planning problem* and *virtual tube passing-through control problem*. For the virtual tube planning problem (Mao and Quan (2022)), a generator curve is first obtained by trajectory planning based on several discrete waypoints, where waypoints are generated from search-based methods. Then the virtual tube is generated by expanding the generator curve but avoiding obstacles. The virtual tube passing-through control problem is solved with a distributed gradient vector field method (Quan et al. (2022, 2023b)) which is often used to control swarm robotics within virtual tubes.

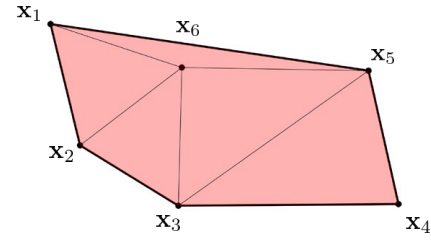


Figure 2. An example of the convex hull. For a set $\mathcal{C} = \{\mathbf{x}_i\}$ ($i = 1, 2, \dots, 6$), the pink area is the $\text{conv } \mathcal{C}$, and the thick black line is $\text{cl } \mathcal{C}$.

In this paper, the definition of the virtual tube is extended into the set and the map in a high-dimension space, which is without a generator curve. Based on the new definition, the optimal virtual tube is proposed for trajectory planning of swarm robotics. And the optimal virtual tube is applied to simulations and experiments, as shown in Fig. 1. The main contributions of this paper are:

- The definition of the virtual tube is extended into a high-dimension space. And the properties of an optimal virtual tube are analyzed, which are suitable for trajectory planning of swarm robotics.
- A linear virtual tube with convex hull terminals is the optimal virtual tube under certain conditions.
- A planning method of the optimal virtual tube is proposed and demonstrated in simulations and experiments.
- An application of the optimal virtual tube is demonstrated in simulations and experiments.

Preliminaries

Convex Optimization (Boyd and Vandenberghe (2004))

Convex hull For a set $\mathcal{C} = \{\mathbf{x}_i\}, i = 1, 2, \dots, q$, the *convex hull* of the set \mathcal{C} , denoted $\text{conv } \mathcal{C}$, is the set of all convex combinations of points in \mathcal{C} :

$$\text{conv } \mathcal{C} = \left\{ \sum_{i=0}^q \theta_i \mathbf{x}_i \mid \mathbf{x}_i \in \mathcal{C}, \theta_i \geq 0, \sum_{i=0}^q \theta_i = 1 \right\}.$$

The *relative interior* of the set \mathcal{C} , denoted $\text{relint } \mathcal{C}$:

$$\text{relint } \mathcal{C} = \{\mathbf{x} \in \mathcal{C} \mid B(\mathbf{x}, r) \cap \mathcal{C} \subseteq \mathcal{C} \text{ for some } r > 0\},$$

where $B(\mathbf{x}, r) = \{\mathbf{y} \mid \|\mathbf{y} - \mathbf{x}\| \leq r\}$, the ball of radius r and center \mathbf{x} in the any norm $\|\cdot\|$. And the closure of \mathcal{C} is expressed as $\text{cl } \mathcal{C}$. An example is shown in Fig. 2.

An optimality criterion for differentiable f_0 Suppose that a convex function f_0 is differentiable, so that for all $\mathbf{x}, \mathbf{y} \in \text{dom } f_0$ (domain of the function f_0),

$$f_0(\mathbf{y}) \geq f_0(\mathbf{x}) + \nabla f_0(\mathbf{x})^T (\mathbf{y} - \mathbf{x}). \quad (1)$$

Let \mathcal{X} denote the feasible set. Then \mathbf{x} is optimal if and only if $\mathbf{x} \in \mathcal{X}$ and

$$\nabla f_0(\mathbf{x})^T (\mathbf{y} - \mathbf{x}) \geq 0, \text{ for all } \mathbf{y} \in \mathcal{X}. \quad (2)$$

Topology

The topological theory is complex and profound. In order to better understand it, we will roughly and intuitively introduce some basic concepts of manifolds that need to be used in the following.

Manifold(Tu (2011)) Intuitively, a manifold is a generalization of curves and surfaces to higher dimensions. It is locally Euclidean in that every point has a neighborhood, called a *chart*, homeomorphic to an open subset of \mathbb{R}^n . The homeomorphism is a bijective and continuous function between topological spaces that has a continuous inverse function.

Diffeomorphism Given two manifolds M and N , a differentiable map $f : M \rightarrow N$ is called a *diffeomorphism* if it is a bijection and its inverse is differentiable as well.

Simple connectivity(Shick (2007)) Intuitively, a space is *simply-connected* if every loop in the space can be shrunk to a point within the space.

Optimal Virtual Tube

A virtual tube is constructed for swarm robotics, which could be used for swarm robotics flow. A generalization of virtual tube is defined as a set in space, and some specific types of the virtual tube including optimal virtual tube are introduced for trajectory planning of swarm robotics.

Virtual tubes

The tube is often used for fluid transportation in three-dimension Euclidean space, which is denoted by \mathbb{R}^3 . However, it is not sufficient to describe a motion of a robot in three-dimension Euclidean space. For example, a set of all affine motions, including rotations and translations in \mathbb{R}^3 , is a six-dimension manifold. But this six-dimension manifold is not \mathbb{R}^6 . Since the virtual tube aims at swarm robotics, it is extended to be defined as a set in n -dimension space.

Intuitively, a virtual tube is constructed by defining maps between two bounded convex sets in space. The convex set is simply connected so that there are no ‘‘holes’’ in the set. The mathematical definition of the virtual tube is formulated in the following.

Definition 1. A *virtual tube* \mathcal{T} , as shown in Fig. 3, is a set in n -dimension space represented by a 4-tuple $(\mathcal{C}_0, \mathcal{C}_1, \mathbf{f}, \mathbf{h})$ where

- $\mathcal{C}_0, \mathcal{C}_1$, called *terminals*, are disjoint bounded convex subsets in n -dimension space.
- \mathbf{f} is a *diffeomorphism*: $\mathcal{C}_0 \rightarrow \mathcal{C}_1$, so that there is a set of order pairs $\mathcal{P} = \{(\mathbf{q}_0, \mathbf{q}_m) \mid \mathbf{q}_0 \in \mathcal{C}_0, \mathbf{q}_m = \mathbf{f}(\mathbf{q}_0) \in \mathcal{C}_1\}$.
- \mathbf{h} is a smooth* map: $\mathcal{P} \times \mathcal{I} \rightarrow \mathcal{T}$ where $\mathcal{I} = [0, 1]$, such that $\mathcal{T} = \{\mathbf{h}((\mathbf{q}_0, \mathbf{q}_m), t) \mid (\mathbf{q}_0, \mathbf{q}_m) \in \mathcal{P}, t \in \mathcal{I}\}$, $\mathbf{h}((\mathbf{q}_0, \mathbf{q}_m), 0) = \mathbf{q}_0$, $\mathbf{h}((\mathbf{q}_0, \mathbf{q}_m), 1) = \mathbf{q}_m$. The function $\mathbf{h}((\mathbf{q}_0, \mathbf{q}_m), t)$ is called a *trajectory* for a order pair $(\mathbf{q}_0, \mathbf{q}_m)$.

And, a *cross-section* \mathcal{C} of a virtual tube at $t \in \mathcal{I}$ is expressed as:

$$\mathcal{C}_t = \{\mathbf{h}((\mathbf{q}_0, \mathbf{q}_m), t) \mid (\mathbf{q}_0, \mathbf{q}_m) \in \mathcal{P}\}. \quad (3)$$

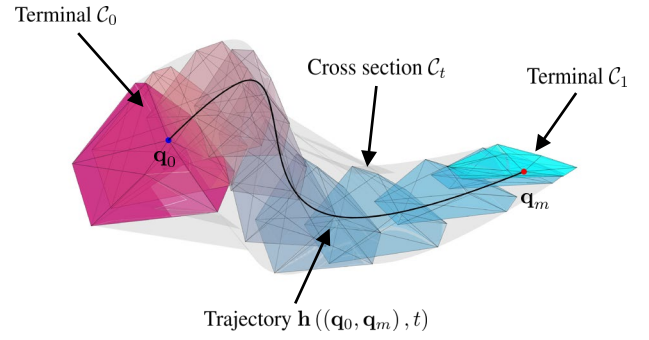


Figure 3. An example of the virtual tube. The purple and blue polyhedrons are terminals. The shaded polyhedrons are cross sections \mathcal{C}_t . The black line is a trajectory that is from \mathbf{q}_0 in terminal \mathcal{C}_0 to \mathbf{q}_m in terminal \mathcal{C}_1 . The gray area is the virtual tube.

The surface of the virtual tube is the boundary of \mathcal{T} , defined as $\partial\mathcal{T}$.

In the following, some properties are directly obtained based on *Definition 1*.

Proposition 1. All cross-sections of a virtual tube are simply connected.

Proof. The convex sets $\mathcal{C}_0, \mathcal{C}_1$ are simply connected. Thus, the order pair \mathcal{P} is simply connected. For a cross-section \mathcal{C}_{t_0} , there is a smooth map \mathbf{h} from $\mathcal{P} \times t_0$ to \mathcal{C}_{t_0} . Therefore, the cross-section is simply connected.

Proposition 2. All cross-sections of a virtual tube are continuous. That is, for every point in the cross-section, there exists at least one trajectory through it.

Proof. The domain $\mathcal{P} \times \mathcal{I}$ is continuous. And the map \mathbf{h} is continuous. So all cross-sections are continuous.

There is no explicit definition of a generator curve, compared with a virtual tube with a generator curve in our previous paper(Mao and Quan (2022)). We use a simple example to show that the previous definition of the virtual tube is a special case of the *Definition 1*.

Suppose \mathcal{T} to be diffeomorphism. Let $\mathcal{C}_0 = \mathcal{T}(s_0, \theta, \rho) = \mathbf{f}_s(\theta, \rho)$, $\mathcal{C}_1 = \mathcal{T}(s_f, \theta, \rho) = \mathbf{f}_f(\theta, \rho)$. Thus, denote $\mathbf{f} = \mathbf{f}_f \circ \mathbf{f}_s^{-1}$ which is a diffeomorphism, and the set of order pairs \mathcal{P} is generated by \mathbf{f} . Then, let $\mathbf{h}((\mathbf{q}_0, \mathbf{q}_m), t) = \mathcal{T}(s_0 + t(s_f - s_0), \theta, \rho)$ which is a smooth map. Therefore, the definition of the virtual tube with a generator curve is a special case of the virtual tube in *Definition 1*. Here is an example.

Example 1. Let a virtual tube with a generator curve shown in Fig. 4 be

$$\mathcal{T}(s, \theta, \rho) = \gamma(s) + \rho \lambda(s, \theta) (\mathbf{n}(s) \cos \theta + \mathbf{b}(s) \sin \theta) \quad (4)$$

where the generator curve $\gamma(s) = [s \ 0 \ 0]^T$, radius $\lambda(s, \theta) = 1$, normal unit vector $\mathbf{n}(s) =$

*A real-valued function is said to be smooth if its derivatives of all orders exist and are continuous.

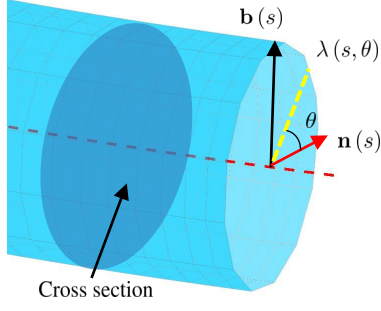


Figure 4. A virtual tube with a generator curve in \mathbb{R}^3 , where the red dotted line is the generator curve; the dark blue plane is a cross-section and the light blue surface is the virtual tube surface.

$\begin{bmatrix} 0 & 1 & 0 \\ 0 & 0 & 1 \end{bmatrix}^T$, binormal unit vector $\mathbf{b}(s) = \begin{bmatrix} 0 & \rho \cos \theta & \rho \sin \theta \end{bmatrix}^T$, $s \in [0, 1]$, $\theta \in [0, 2\pi)$, $\rho \in [0, 1]$. Let $\mathcal{C}_0 = \mathcal{T}(0, \theta, \rho) = \begin{bmatrix} 0 & \rho \cos \theta & \rho \sin \theta \end{bmatrix}^T$, $\mathcal{C}_1 = \mathcal{T}(1, \theta, \rho) = \begin{bmatrix} 1 & \rho \cos \theta & \rho \sin \theta \end{bmatrix}^T$. Obviously, \mathcal{C}_0 and \mathcal{C}_1 are disjoint bounded convex subsets, and are called terminals. For $\mathbf{q}_0 = \begin{bmatrix} 0 & \rho \cos \theta & \rho \sin \theta \end{bmatrix}^T \in \mathcal{C}_0$, $\mathbf{f}(\mathbf{q}_0) = \mathbf{q}_m = \begin{bmatrix} 1 & \rho \cos \theta & \rho \sin \theta \end{bmatrix}^T \in \mathcal{C}_1$. Thus, \mathbf{f} is a diffeomorphism and then a set of order pairs \mathcal{P} is constructed. Let $\mathbf{h}((\mathbf{q}_0, \mathbf{q}_m), t) = \mathcal{T}(t, \theta, \rho)$ which is a diffeomorphism. Therefore, this virtual tube with a generator curve is a special case of the virtual tube defined in this paper.

Some useful types of virtual tubes are defined in the following.

Definition 2. A virtual tube $\mathcal{T}(\mathcal{C}_0, \mathcal{C}_1, \mathbf{f}, \mathbf{h})$ is *linear* if it satisfies following properties:

- The diffeomorphism \mathbf{f} is a *linear* map for any $\mathbf{q}_{0,k} \in \mathcal{C}_0$ and $\theta_k \in \mathbb{R}$, namely

$$\mathbf{f}\left(\sum_{k=1}^q \theta_k \mathbf{q}_{0,k}\right) = \sum_{k=1}^q \theta_k \mathbf{f}(\mathbf{q}_{0,k}).$$

- The smooth map \mathbf{h} is a *linear* map for any $(\mathbf{q}_{0,k}, \mathbf{q}_{m,k}) \in \mathcal{P}$ and $\eta_k \in \mathbb{R}$, namely

$$\begin{aligned} \mathbf{h}\left(\sum_{k=1}^q \eta_k (\mathbf{q}_{0,k}, \mathbf{q}_{m,k}), t\right) \\ = \sum_{k=1}^q \eta_k \mathbf{h}((\mathbf{q}_{0,k}, \mathbf{q}_{m,k}), t). \end{aligned}$$

Definition 3. A terminal \mathcal{C}_0 (or \mathcal{C}_1) is a *convex hull* of the finite set $\{\mathbf{q}_{0,k}\}$ if it can be expressed as

$$\mathcal{C}_0 = \left\{ \mathbf{q}_0 \mid \mathbf{q}_0 = \sum_{k=1}^q \theta_k \mathbf{q}_{0,k}, \sum_{k=1}^q \theta_k = 1, \theta_k \geq 0 \right\}. \quad (5)$$

Optimal virtual tube

Before defining the optimal virtual tube, the optimal trajectory is needed to be defined. A cost function related with trajectory \mathbf{h} is defined as $g(\mathbf{h}((\mathbf{q}_0, \mathbf{q}_m), t))$.

Definition 4. A trajectory \mathbf{h}^* for a order pair $(\mathbf{q}_0, \mathbf{q}_m) \in \mathcal{P}$ is *optimal* with respect to cost g if

$$\mathbf{h}^* = \arg \min_{\mathbf{h} \in \mathcal{H}} g(\mathbf{h}((\mathbf{q}_0, \mathbf{q}_m), t))$$

where $t \in \mathcal{I}$ and \mathcal{H} is a candidate trajectory set.

Consequently, the definition of an optimal virtual tube is proposed in the following.

Definition 5. A virtual tube \mathcal{T} is *optimal* with respect to a cost g if every trajectory in the tube is *optimal* with respect to a cost g , namely $\mathcal{T} = (\mathcal{C}_0, \mathcal{C}_1, \mathbf{f}, \mathbf{h}^*)$.

As shown in Fig 3, if all trajectories in the tube are optimal, the tube is an optimal virtual tube.

A Type of Optimal Virtual Tube: Linear Virtual Tube with Convex Hull Terminals

There are infinite trajectories in the virtual tube, so it is impossible to solve optimization problems for every optimal trajectory respectively. The natural first idea is interpolation to reduce calculation significantly. There are lemmas about optimal conditions shown in *Appendix A*, which are useful for constructing a type of optimal virtual tube.

Lemma 1. Constrained with hyperplanes: Suppose that a convex optimization problem has the following type

$$\begin{aligned} \min \quad & f_0(\mathbf{x}) \\ \text{s.t.} \quad & \mathbf{A}\mathbf{x} = \mathbf{b} \end{aligned} \quad (6)$$

where $f_0(\mathbf{x})$ is a convex function with respect to $\mathbf{x} = [x_0 \ x_1 \ \dots \ x_n]^T$, $\mathbf{A} \in \mathbb{R}^{p \times (n+1)}$ ($p < n+1$), $\mathbf{b} \in \mathbb{R}^p$ and $\nabla f_0(\mathbf{x})$ is linear with respect to \mathbf{x} . The optimal solution \mathbf{x}_k is obtained when $\mathbf{b} = \mathbf{b}_k$. Denote $\mathcal{B} = \{\mathbf{b}_k\}$, $\mathcal{X} = \{\mathbf{x}_k\}$, $k = 1, 2, \dots, q$, $\mathbf{b}(\boldsymbol{\theta}) = \sum_{k=0}^q \theta_k \mathbf{b}_k \in \mathbf{conv} \mathcal{B}$. Then $\mathbf{x}(\boldsymbol{\theta}) = \sum_{k=0}^q \theta_k \mathbf{x}_k \in \mathbf{conv} \mathcal{X}$ is feasible and optimal.

Lemma 2. Standard form: Suppose that a convex optimization problem has the following type

$$\begin{aligned} \min \quad & f_0(\mathbf{x}) \\ \text{s.t.} \quad & \mathbf{A}\mathbf{x} = \mathbf{b} \\ & f_i(\mathbf{x}) \leq 0, i = 1, \dots, n_c \end{aligned} \quad (7)$$

where $f_i(\mathbf{x})$ ($i = 0, 1, \dots, n_c$) are convex functions with respect to $\mathbf{x} = [x_0 \ x_1 \ \dots \ x_n]^T$, $\mathbf{A} \in \mathbb{R}^{p \times (n+1)}$ ($p < n+1$), $\mathbf{b} \in \mathbb{R}^p$ and $\nabla f_0(\mathbf{x})$ is linear with respect to \mathbf{x} . The optimal solution \mathbf{x}_k is obtained when $\mathbf{b} = \mathbf{b}_k$. Denote $\mathcal{B} = \{\mathbf{b}_k\}$, $\mathcal{X} = \{\mathbf{x}_k\}$, $k = 1, 2, \dots, q$, $\mathbf{b}(\boldsymbol{\theta}) = \sum_{k=0}^q \theta_k \mathbf{b}_k \in \mathbf{conv} \mathcal{B}$. Then $\mathbf{x}(\boldsymbol{\theta}) = \sum_{k=0}^q \theta_k \mathbf{x}_k \in \mathbf{conv} \mathcal{X}$ is feasible and optimal.

Definition 6. A virtual tube $\mathcal{T}(\mathcal{C}_0, \mathcal{C}_1, \mathbf{f}, \mathbf{h})$ is called a *linear virtual tube with convex hull terminals* if it satisfies:

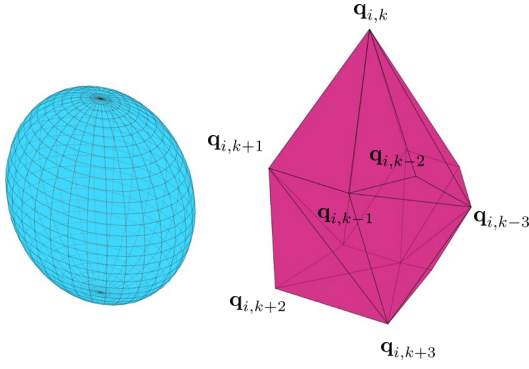


Figure 5. The blue sphere is a terminal which is a convex set. The purple polyhedron is a convex hull terminal. And they could also indicate the cross-section C_t at t .

- The terminal C_0 is the convex hull of the finite set $\{\mathbf{q}_{0,k}\}$, and the terminal C_1 is the convex hull of the finite set $\{\mathbf{q}_{m,k}\}$. The set $\{\mathbf{q}_{0,k}\}$ and the set $\{\mathbf{q}_{m,k}\}$ have the same number of elements.
- For any $\mathbf{q}_{0,k}$ in the set $\{\mathbf{q}_{0,k}\}$, $\mathbf{q}_{m,k} = \mathbf{f}(\mathbf{q}_{0,k})$.
- The virtual tube $\mathcal{T}(C_0, C_1, \mathbf{f}, \mathbf{h})$ is linear.

The linear virtual tube with convex hull terminals is a special case of the virtual tube, for the convex hull of the finite set is a polyhedron (Boyd and Vandenberghe (2004)), as shown in Fig. 5. An example of the linear virtual tube with convex hull terminals is shown in Fig. 3.

Theorem 1. A linear virtual tube with convex hull terminals $\mathcal{T}(C_0, C_1, \mathbf{f}, \mathbf{h})$ is optimal with respect to cost f_0 if (i) its trajectory for each order pair $(\mathbf{q}_0, \mathbf{q}_m)$ can be linearly parameterized as $\mathbf{h}((\mathbf{q}_0, \mathbf{q}_m), t) = \mathbf{C}(t) \mathbf{x}$ where $\mathbf{C}(t)$ is a matrix only respect to t , and \mathbf{x} is a parameter vector, (ii) the trajectories $\mathbf{h}((\mathbf{q}_{0,k}, \mathbf{q}_{m,k}), t)$ for order pairs $(\mathbf{q}_{0,k}, \mathbf{q}_{m,k})$ ($k = 1, 2, \dots, q$) are optimal with respect to cost f_0 and satisfy the conditions in (7), where $\mathbf{b} = \mathbf{b}_k, \mathbf{x} = \mathbf{x}_k$ for each trajectory $\mathbf{h}((\mathbf{q}_{0,k}, \mathbf{q}_{m,k}), t)$, (iii) The linear equality constraint is $\mathbf{A}\mathbf{x} = \sum_{k=1}^q \theta_k \mathbf{b}_k$ for each order pair $(\mathbf{q}_0, \mathbf{q}_m)$.

Proof. We show that in *Step 1* any trajectory $\mathbf{h}((\mathbf{q}_0, \mathbf{q}_m), t)$ in the linear virtual tube with convex hull terminals can be expressed as the affine combination of trajectories $\mathbf{h}((\mathbf{q}_{0,k}, \mathbf{q}_{m,k}), t)$. Then, in *Step 2*, we will show that any trajectory $\mathbf{h}((\mathbf{q}_0, \mathbf{q}_m), t)$ is optimal which is derived by *Lemma 2*. Therefore, this virtual tube is optimal.

Step 1. Suppose the terminal C_0 is the convex hull of the finite set $\{\mathbf{q}_{0,k}\}$, such as

$$C_0 = \left\{ \mathbf{q}_0 \mid \mathbf{q}_0 = \sum_{k=1}^q \theta_k \mathbf{q}_{0,k}, \sum_{k=1}^q \theta_k = 1, \theta_k \geq 0 \right\},$$

where q is the number of the elements in set $\{\mathbf{q}_{0,k}\}$. Then q order pairs $\{(\mathbf{q}_{0,k}, \mathbf{q}_{m,k})\}$ are constructed by

$$\mathbf{q}_{m,k} = \mathbf{f}(\mathbf{q}_{0,k}).$$

Thus, the set of order pairs \mathcal{P} is constructed by

$$\begin{aligned} \mathcal{P} &= \{(\mathbf{q}_0, \mathbf{f}(\mathbf{q}_m))\} = \left\{ \left(\sum_{k=1}^q \theta_k \mathbf{q}_{0,k}, \mathbf{f} \left(\sum_{k=1}^q \theta_k \mathbf{q}_{0,k} \right) \right) \right\} \\ &= \left\{ \left(\sum_{k=1}^q \theta_k \mathbf{q}_{0,k}, \sum_{k=1}^q \theta_k \mathbf{f}(\mathbf{q}_{0,k}) \right) \right\} \\ &= \left\{ \left(\sum_{k=1}^q \theta_k \mathbf{q}_{0,k}, \sum_{k=1}^q \theta_k \mathbf{q}_{m,k} \right) \right\} \\ &= \left\{ \sum_{k=1}^q \theta_k (\mathbf{q}_{0,k}, \mathbf{q}_{m,k}) \right\}. \end{aligned}$$

Through solving optimization problem in (7), the q optimal trajectories for order pairs $\{(\mathbf{q}_{0,k}, \mathbf{q}_{m,k})\}$ are generated, which are linearly parameterized as

$$\mathbf{h}^*((\mathbf{q}_{0,k}, \mathbf{q}_{m,k}), t) = \mathbf{C}(t) \mathbf{x}_k, k = 1, \dots, q, \quad (8)$$

where $\mathbf{C}(t)$ is a matrix with t , \mathbf{x}_k is the optimal solution.

Thus, any trajectory for the order pair in \mathcal{P} is expressed as

$$\begin{aligned} \mathbf{h}((\mathbf{q}_0, \mathbf{q}_m), t) &= \mathbf{h} \left(\sum_{k=1}^q \theta_k (\mathbf{q}_{0,k}, \mathbf{q}_{m,k}), t \right) \\ &= \sum_{k=1}^q \theta_k \mathbf{h}^*((\mathbf{q}_{0,k}, \mathbf{q}_{m,k}), t) \\ &= \sum_{k=1}^q \theta_k \mathbf{C}(t) \mathbf{x}_k = \mathbf{C}(t) \sum_{k=1}^q \theta_k \mathbf{x}_k. \end{aligned} \quad (9)$$

And, the linear equality constraint in (7) is expressed as

$$\mathbf{A}\mathbf{x} = \sum_{k=1}^q \theta_k \mathbf{b}_k. \quad (10)$$

Step 2. We will show that any trajectory in the linear virtual tube with convex hull terminals is optimal, namely this virtual tube is optimal.

Because \mathbf{x}_k of the optimal trajectory $\mathbf{h}^*((\mathbf{q}_{0,k}, \mathbf{q}_{m,k}), t)$ is the optimal solution in (7) where $\mathbf{b} = \mathbf{b}_k$, according to *Lemma 2* and (10), $\mathbf{x} = \sum_{k=1}^q \theta_k \mathbf{x}_k$ is the optimal solution. Therefore, any trajectory for order pair $(\mathbf{q}_0, \mathbf{q}_m) \in \mathcal{P}$ is optimal which is expressed as

$$\begin{aligned} \mathbf{h}^*((\mathbf{q}_0, \mathbf{q}_m), t) &= \mathbf{C}(t) \mathbf{x} = \mathbf{C}(t) \sum_{k=1}^q \theta_k \mathbf{x}_k \\ &= \sum_{k=1}^q \theta_k \mathbf{C}(t) \mathbf{x}_k = \sum_{k=1}^q \theta_k \mathbf{h}^*((\mathbf{q}_{0,k}, \mathbf{q}_{m,k}), t). \end{aligned}$$

Thus, this linear virtual tube with convex hull terminals $(C_0, C_1, \mathbf{f}, \mathbf{h}^*)$ is optimal.

An example of the optimal linear virtual tube with convex hull terminals is in the following.

Example 2. In two-dimension Euclidean space, suppose that there exists a linear virtual tube with convex hull terminals $\mathcal{T}(C_0, C_1, \mathbf{f}, \mathbf{h})$. The terminals C_0, C_1 are expressed as the convex hull of the the set $\{\mathbf{q}_{0,1}, \mathbf{q}_{0,2}\}$ and $\{\mathbf{q}_{m,1}, \mathbf{q}_{m,2}\}$, namely $C_0 = \mathbf{q}_0(\theta) = (1 - \theta) \mathbf{q}_{0,1} + \theta \mathbf{q}_{0,2}, C_1 = \mathbf{q}_m(\theta) = (1 - \theta) \mathbf{q}_{m,1} + \theta \mathbf{q}_{m,2}, \theta \in [0, 1]$. The smooth map \mathbf{f} is defined as $\mathbf{q}_{m,k} = \mathbf{f}(\mathbf{q}_{0,k}), k = 1, 2$. Thus, a set of order pairs is expressed as $\mathcal{P} = \{(\mathbf{q}_0(\theta), \mathbf{q}_m(\theta))\}$. Let $\mathbf{h}_0^*(t), \mathbf{h}_1^*(t)$ denote the optimal trajectories for order pairs $(\mathbf{q}_{0,1}, \mathbf{q}_{m,1})$ and $(\mathbf{q}_{0,2}, \mathbf{q}_{m,2})$ respectively which are generated by solving optimization problems satisfying *Lemma 2*. And the linear equality constraint for $(\mathbf{q}_0(\theta), \mathbf{q}_m(\theta))$

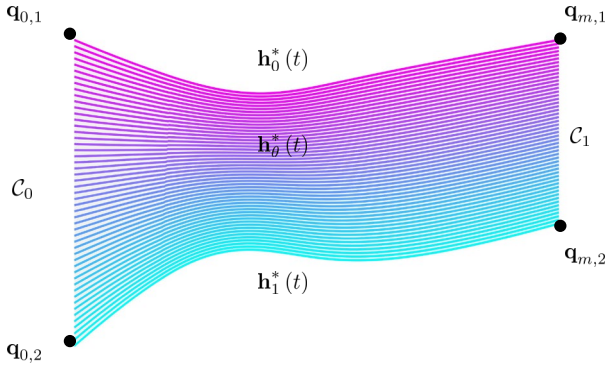


Figure 6. An optimal virtual tube example. Different colors represent different optimal trajectories. Curves $\mathbf{h}_0^*(t)$ and $\mathbf{h}_1^*(t)$ are optimal trajectories generated by solving optimization problems. And $\mathbf{h}_\theta^*(t)$ are optimal trajectories generated by interpolation.

satisfy the condition (iii) in *Theorem 1*. Thus, the optimal trajectory of any order pair $(\mathbf{q}_0(\theta), \mathbf{q}_m(\theta)) \in \mathcal{P}$ is expressed as $\mathbf{h}_\theta^*(t) = (1 - \theta)\mathbf{h}_0^*(t) + \theta\mathbf{h}_1^*(t)$. Since every trajectory in virtual tube is optimal, $\mathcal{T}(\mathcal{C}_0, \mathcal{C}_1, \mathbf{f}, \mathbf{h}^*)$ is the optimal virtual tube, as shown in Fig. 6.

A Planning Method to Obtain An Optimal Virtual Tube

Considering a robot swarm composed of M agents labeled by $j \in \mathcal{M} = \{1, \dots, M\}$, a start area which is the convex hull of set $\{\mathbf{q}_{0,k}\}$ is labeled by \mathcal{C}_0 , and a goal area which is the convex hull of set $\{\mathbf{q}_{m,k}\}$ is labeled by \mathcal{C}_1 . Suppose that the start position $\mathbf{q}_0(\theta_j) \in \mathcal{C}_0$ of robot j is given. There is an obstacle-dense environment between the start area and the goal area. The objective is to construct an optimal virtual tube and make robots pass through the obstacle-dense environment in the optimal virtual tube.

Outline

For an optimal virtual tube $\mathcal{T}(\mathcal{C}_0, \mathcal{C}_1, \mathbf{f}, \mathbf{h}^*)$, the set of order pairs \mathcal{P} is constructed by \mathbf{f} first, after inputting terminals \mathcal{C}_0 and \mathcal{C}_1 . Then the paths for order pairs $(\mathbf{q}_{0,k}, \mathbf{q}_{m,k})$ are found. Next, the optimal trajectories $\mathbf{h}^*((\mathbf{q}_{0,k}, \mathbf{q}_{m,k}), t)$ for order pairs $(\mathbf{q}_{0,k}, \mathbf{q}_{m,k})$ are generated by solving optimization problems. Finally, an optimal linear virtual tube with convex hull terminals $\mathcal{T}(\mathcal{C}_0, \mathcal{C}_1, \mathbf{f}, \mathbf{h}^*)$ is constructed, with an infinite number of optimal trajectories. The whole process of optimal virtual tube planning is shown in Fig. 7.

Constructing order pairs

Suppose that the start area and goal area, called terminal \mathcal{C}_0 and \mathcal{C}_1 , are the convex hull of $\{\mathbf{q}_{0,k}\}$ and $\{\mathbf{q}_{m,k}\}$ respectively. The order pairs \mathcal{P} are constructed from a map \mathbf{f} .

Any start position $\mathbf{q}_0(\theta_j)$ in terminal \mathcal{C}_0 is expressed as

$$\mathbf{q}_0(\theta_j) = \sum_{k=1}^q \theta_{kj} \mathbf{q}_{0,k}, \quad \sum_{k=1}^q \theta_{kj} = 1, \theta_{kj} \geq 0, j \in \mathbb{Z}^+, \quad (11)$$

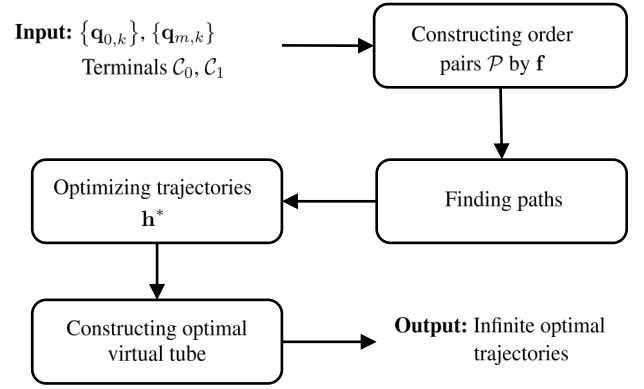


Figure 7. The process of the optimal virtual tube planning.

where q is a finite number of elements in $\{\mathbf{q}_{0,k}\}$. Compared with the infinite number of start positions in terminal \mathcal{C}_0 , the number of elements in $\{\mathbf{q}_{0,k}\}$ is small enough. Let \mathbf{f} be the map between \mathcal{C}_0 and \mathcal{C}_1 so that for any goal position $\mathbf{q}_m(\theta_j) \in \mathcal{C}_1$,

$$\begin{aligned} \mathbf{q}_m(\theta_j) &= \mathbf{f}(\mathbf{q}_0(\theta_j)) = \mathbf{f}\left(\sum_{k=1}^q \theta_{kj} \mathbf{q}_{0,k}\right) = \sum_{k=1}^q \theta_{kj} \mathbf{f}(\mathbf{q}_{0,k}) \\ &= \sum_{k=1}^q \theta_{kj} \mathbf{q}_{m,k}. \end{aligned}$$

The set of order pairs \mathcal{P} , thus, has been constructed, such as $\{(\mathbf{q}_0(\theta_j), \mathbf{q}_m(\theta_j))\}$.

Finding paths

The paths for order pairs $(\mathbf{q}_{0,k}, \mathbf{q}_{m,k})$ ($k = 1, \dots, q$) are needed to be found after constructing order pairs. And a normalized parameterization of the paths is designed.

There are many path finding methods used for find waypoints in the obstacle environment such as RRT, RRT* (Karaman and Frazzoli (2011)), and A*. For each order pair $(\mathbf{q}_{0,k}, \mathbf{q}_{m,k})$ ($k = 1, \dots, q$), we select RRT* to find $m + 1$ waypoints $\{\mathbf{q}_{i,k}\}$ ($i = 0, \dots, m$) between $\mathbf{q}_{0,k}$ and $\mathbf{q}_{m,k}$.

To parameterize the waypoints $\{\mathbf{q}_{i,k}\}$, parameters $u_{i,k}$ are assigned to corresponding waypoint $\mathbf{q}_{i,k}$. Thus, a partition of u_k is first designed, called knots $\{u_{i,k}\}$. Then public knots $\{u_i\}$ and public normalized knots $\{t_k\}$ are generated by domain transformation. The chord length parameterization, a suitable method in most engineering applications (Piegl and Tiller (2000)), is used to generate knots $\{u_{i,k}\}$ which are expressed as

$$u_{i,k} = \begin{cases} 0, & i = 0, \\ u_{i-1,k} + \|\mathbf{q}_{i,k} - \mathbf{q}_{i-1,k}\|, & i = 1, 2, \dots, m. \end{cases} \quad (12)$$

It should be noted that the knots $\{u_{i,k}\}$ for each pair $(\mathbf{q}_{0,k}, \mathbf{q}_{m,k})$ are generally not the same, because of variation of distances $\|\mathbf{q}_{i,k} - \mathbf{q}_{i-1,k}\|$, $k = 1, \dots, q$. Motivated by the parameterization of tensor product surface (Strothotte and Schlechtweg (2002)), all parameterizations of paths are expected to be the same for convenience. The public knots $\{u_i\}$ is the arithmetic mean of all knots, which is expressed as

$$u_i = \frac{\sum_{k=1}^q u_{ki}}{q}. \quad (13)$$

To get the normalized parameterization for correspondence with the *Definition 1*, the normalized knots $\{t_i\}$ is obtained by

$$t_i = \frac{u_i}{u_m}, i = 0, 1, \dots, m. \quad (14)$$

Connecting adjacent waypoints with straight lines, the RRT* path planner finds q collision-free paths for q order pairs $\{\mathbf{q}_{0,k}, \mathbf{q}_{m,k}\}$ respectively.

Remark 1. The numbers of the waypoints $\{\mathbf{q}_{i,k}\}$ of different order pairs are assumed as the same. Otherwise, different numbers of the waypoints $\{\mathbf{q}_{i,k}\}$ lead to different lengths of parameter vectors \mathbf{x} in *Theorem 1*, that would not satisfy *Lemmas 1,2*. And all paths are homotopic, so that there is no obstacle between paths.

Optimizing trajectories

The original paths in the above subsection have some sharp corners, as shown in Fig. 15(b), which are not suitable for the dynamics of the robot. It is necessary to further find smooth trajectories based on the original paths.

Trajectory representation There are many ways to represent trajectories linearly, such as B-spline and polynomials. It is convenient to use n orders piecewise polynomial to represent the trajectory \mathbf{h} , such as

$$\mathbf{h}(t) = \begin{cases} \sum_{i=0}^n \mathbf{a}_{i,1} t^i & t_0 < t < t_1 \\ \sum_{i=0}^n \mathbf{a}_{i,2} t^i & t_1 < t < t_2 \\ \vdots & \vdots \\ \sum_{i=0}^n \mathbf{a}_{i,m} t^i & t_{m-1} < t < t_m \end{cases} \quad (15)$$

where $\mathbf{a}_{i,j} = [a_{1,i,j} \ a_{2,i,j} \ \dots \ a_{d,i,j}]^T \in \mathbb{R}^d$. For any $t \in [t_{k-1}, t_k]$, the trajectory $\mathbf{h}(t)$ could be represented by matrix

$$\mathbf{h}_k(t) = \mathbf{C}(t) \mathbf{x}_k \quad (16)$$

where $\mathbf{C}(t) = [\mathbf{I}_d \ t\mathbf{I}_d \ t^2\mathbf{I}_d \ \dots \ t^n\mathbf{I}_d]$,

$$\mathbf{x}_k = \begin{bmatrix} \mathbf{a}_{0,k} \\ \mathbf{a}_{1,k} \\ \mathbf{a}_{2,k} \\ \vdots \\ \mathbf{a}_{n,k} \end{bmatrix}.$$

The representation of trajectory (16) is convenient to be used in a quadratic program (QP) in the following.

Constraints The constraints, including the terminal conditions and intermediate conditions, are constructed as linear equations for smoothing. For obstacle avoidance, adding corridor constraints could avoid collision.

The terminal conditions are expressed as

$$\begin{aligned} \mathbf{h}_1(t_0) &= \mathbf{C}(t_0) \mathbf{x}_1 = \mathbf{q}_{0,k}, \\ \mathbf{h}_m(t_m) &= \mathbf{C}(t_m) \mathbf{x}_m = \mathbf{q}_{m,k}, \\ \left. \frac{d^p \mathbf{h}_1(t)}{dt^p} \right|_{t=t_0} &= \mathbf{q}_{0,k}^{(p)}, \\ \left. \frac{d^p \mathbf{h}_m(t)}{dt^p} \right|_{t=t_m} &= \mathbf{q}_{m,k}^{(p)}, \end{aligned} \quad (17)$$

where $\mathbf{q}_{0,k}^{(p)}$ and $\mathbf{q}_{m,k}^{(p)}$ are the p -order conditions in the start and goal points, the terminals of the trajectory are constrained in start and goal points. And the intermediate conditions are expressed as

$$\left. \frac{d^p \mathbf{h}_i(t)}{dt^p} \right|_{t=t_i} = \left. \frac{d^p \mathbf{h}_{i+1}(t)}{dt^p} \right|_{t=t_i}, \quad (18)$$

where $p = 0, 1, 2, \dots, k_r, i = 1, 2, \dots, m-1$,

$$\begin{aligned} \left. \frac{d^p \mathbf{h}_i(t)}{dt^p} \right|_{t=t_i} &= \left. \frac{d^p \mathbf{C}(t)}{dt^p} \right|_{t=t_i} \mathbf{x}_i, \\ \left. \frac{d^p \mathbf{h}_{i+1}(t)}{dt^p} \right|_{t=t_i} &= \left. \frac{d^p \mathbf{C}(t)}{dt^p} \right|_{t=t_i} \mathbf{x}_{i+1}. \end{aligned}$$

Specifically, when $p = 0$, the terminals of each segment are waypoints:

$$\mathbf{h}_i(t_i) = \mathbf{h}_{i+1}(t_i) = \mathbf{q}_{i,k}. \quad (19)$$

For convenience, we denote

$$\mathbf{C}_t^{(p)} = \frac{d^p \mathbf{C}(t)}{dt^p}$$

which could transform (18) into

$$\begin{bmatrix} \mathbf{C}_{t_i}^{(p)} & -\mathbf{C}_{t_{i+1}}^{(p)} \end{bmatrix} \begin{bmatrix} \mathbf{x}_i \\ \mathbf{x}_{i+1} \end{bmatrix} = \mathbf{0}. \quad (20)$$

Based on (17), (19), and (20), the linear equality constraints are derived

$$\mathbf{A} \mathbf{x} = \begin{bmatrix} \mathbf{A}_1 \\ \mathbf{A}_2 \\ \mathbf{A}_3 \end{bmatrix} \mathbf{x} = \begin{bmatrix} \mathbf{b}_1 \\ \mathbf{b}_2 \\ \mathbf{b}_3 \end{bmatrix}_k = \mathbf{b}_k, \quad (21)$$

where

$$\mathbf{x} = \begin{bmatrix} \mathbf{x}_1 \\ \vdots \\ \mathbf{x}_m \end{bmatrix}, \mathbf{b}_1 = \begin{bmatrix} \mathbf{0} \\ \vdots \\ \mathbf{0} \end{bmatrix}, \mathbf{b}_2 = \begin{bmatrix} \mathbf{q}_{0,k} \\ \mathbf{q}_{1,k} \\ \vdots \\ \mathbf{q}_{m-1,k} \\ \mathbf{q}_{m,k} \end{bmatrix},$$

$$\mathbf{b}_3 = \begin{bmatrix} \mathbf{q}_{0,k}^{(p)} & \dots & \mathbf{q}_{0,k}^{(1)} & \mathbf{q}_{m,k}^{(p)} & \dots & \mathbf{q}_{m,k}^{(1)} \end{bmatrix}^T,$$

$$\mathbf{A}_1 = \begin{bmatrix} \mathbf{C}_{t_1}^{(p)} & -\mathbf{C}_{t_1}^{(p)} & \dots & \mathbf{0} & \mathbf{0} \\ \vdots & \vdots & \dots & \vdots & \vdots \\ \mathbf{0} & \mathbf{0} & \dots & \mathbf{C}_{t_{m-1}}^{(p)} & -\mathbf{C}_{t_{m-1}}^{(p)} \end{bmatrix},$$

$$\mathbf{A}_2 = \begin{bmatrix} \mathbf{C}_{t_0} & \mathbf{0} & \dots & \mathbf{0} \\ \mathbf{0} & \mathbf{C}_{t_1} & \dots & \mathbf{0} \\ \vdots & \vdots & \ddots & \vdots \\ \mathbf{0} & \mathbf{0} & \dots & \mathbf{C}_{t_{m-1}} \\ \mathbf{0} & \mathbf{0} & \dots & \mathbf{C}_{t_m} \end{bmatrix},$$

$$\mathbf{A}_3 = \begin{bmatrix} \mathbf{C}_{t_0}^{(p)} & \mathbf{0} & \dots & \mathbf{0} & \mathbf{0} \\ \vdots & \vdots & \ddots & \vdots & \vdots \\ \mathbf{C}_{t_0}^{(1)} & \mathbf{0} & \dots & \mathbf{0} & \mathbf{0} \\ \mathbf{0} & \mathbf{0} & \dots & \mathbf{0} & \mathbf{C}_{t_m}^{(p)} \\ \vdots & \vdots & \ddots & \mathbf{0} & \vdots \\ \mathbf{0} & \mathbf{0} & \dots & \mathbf{0} & \mathbf{C}_{t_m}^{(1)} \end{bmatrix}.$$

In order to avoid collision between trajectories and obstacles, corridor constraints (Mellinger and Kumar (2011)) are added by constraining n_j intermediate points in the segment from $\mathbf{q}_{i,k}$ to $\mathbf{q}_{i+1,k}$. For an intermediate point of trajectory $\mathbf{h}(s_j)$ in the segment from $\mathbf{q}_{i,k}$ to $\mathbf{q}_{i+1,k}$, the perpendicular distance vector between $\mathbf{h}(s_j)$ and the segment is expressed as

$$\mathbf{d}_i(s_j) = (\mathbf{h}(s_j) - \mathbf{q}_{i,k}) - ((\mathbf{h}(s_j) - \mathbf{q}_{i,k}) \cdot \mathbf{t}_i) \mathbf{t}_i,$$

where \mathbf{t}_i is the unit vector along segment from $\mathbf{q}_{i,k}$ to $\mathbf{q}_{i+1,k}$. Thus, the convex constraints are expressed as:

$$f_i(\mathbf{x}) = |\mathbf{h}^T(s_j) \mathbf{d}_i(s_j)| - \delta_i \leq 0, \quad (22)$$

where $s_j = t_i + \frac{j}{1+n_i}(t_{i+1} - t_i)$, $i = 1, \dots, n_c$, $j = 1, \dots, n_j$, δ_i is the corridor width, $\mathbf{d}_i(s_j)$ is the perpendicular distance vector.

Cost function The optimization problem to minimize energy cost could be solved as a QP by regarding \mathbf{x} in (21) as variable vectors (Mellinger and Kumar (2011)). The cost function is expressed as

$$\begin{aligned} E_s &= \int_{t_0}^{t_m} \left\| \frac{d^{k_r} \mathbf{h}(t)}{dt^{k_r}} \right\|^2 dt \\ &= \sum_{i=1}^m \mathbf{x}_i^T \int_{t_{i-1}}^{t_i} \mathbf{C}_t^{(k_r)T} \mathbf{C}_t^{(k_r)} dt \mathbf{x}_i \\ &= \mathbf{x}^T \mathbf{H} \mathbf{x}. \end{aligned} \quad (23)$$

Optimization problem The goal of the optimization problem is to minimize the energy cost meanwhile satisfying constraints. Thus, combining (21), (22), and (23), this problem could be expressed as

$$\begin{aligned} \min_{\mathbf{x}} \quad & \mathbf{x}^T \mathbf{H} \mathbf{x} \\ \text{s.t.} \quad & \mathbf{A} \mathbf{x} = \mathbf{b}_k \\ & f_i(\mathbf{x}) \leq 0, i = 1, \dots, n_c, \end{aligned} \quad (24)$$

which is the form in Lemma 2. Therefore, the optimal trajectories $\mathbf{h}^*((\mathbf{q}_{0,k}, \mathbf{q}_{m,k}), t)$ are derived by solving q optimization problems for q order pairs $\{(\mathbf{q}_{0,k}, \mathbf{q}_{m,k})\}$.

Constructing optimal virtual tube

The waypoints for any order pair $(\mathbf{q}_0(\theta_j), \mathbf{q}_m(\theta_j))$ could be expressed as

$$\mathbf{q}_i(\theta_j) = \sum_{k=1}^q \theta_{kj} \mathbf{q}_{i,k}, i = 0, 1, 2, \dots, m.$$

And the normalized knots $\{t_i\}$ is used to parameterize the waypoints. Thus, the linear equality constraints are expressed as

$$\begin{bmatrix} \mathbf{A}_1 \\ \mathbf{A}_2 \\ \mathbf{A}_3 \end{bmatrix} \mathbf{x} = \sum_{k=1}^q \theta_{kj} \begin{bmatrix} \mathbf{b}_1 \\ \mathbf{b}_2 \\ \mathbf{b}_3 \end{bmatrix}_k. \quad (25)$$

According to Theorem 1, the linear virtual tube with convex hull terminals $(\mathcal{C}_0, \mathcal{C}_1, \mathbf{f}, \mathbf{h}^*)$ is optimal. In other words, for any start point $\mathbf{q}_0(\theta_j)$, the goal point $\mathbf{q}_m(\theta_j)$ is assigned, and then the optimal trajectory $\mathbf{h}^*((\mathbf{q}_0(\theta_j), \mathbf{q}_m(\theta_j)), t)$ is expressed as

$$\mathbf{h}^*((\mathbf{q}_0(\theta_j), \mathbf{q}_m(\theta_j)), t) = \sum_{k=1}^q \theta_{kj} \mathbf{h}^*((\mathbf{q}_{0,k}, \mathbf{q}_{m,k}), t), \quad (26)$$

where $\sum_{k=1}^q \theta_{kj} = 1, \theta_{kj} \geq 0$.

Model Predictive Control for Tracking Trajectories in An Optimal Virtual Tube

A hierarchical approach is employed to enable swarm robotics moving within the optimal virtual tube, comprising two layers: optimal virtual tube planning and trajectory tracking for a robot swarm. First, the optimal virtual tube planning is proposed in above section, which generates optimal trajectories for the swarm. Subsequently, each robot tracks its own trajectory while avoiding collisions with other robots. This section first introduces a robot model and then designs a Model Predictive Control (MPC) controller to track trajectory and avoid conflicts.

Robot Model

The dynamics of a holonomic robot is described by a mass point model:

$$\begin{aligned} \dot{\mathbf{p}}_i &= \mathbf{v}_i, \\ \dot{\mathbf{v}}_i &= \mathbf{u}_i, \end{aligned} \quad (27)$$

where $\mathbf{p}_i \in \mathbb{R}^2$ (\mathbb{R}^3) and $\mathbf{v}_i \in \mathbb{R}^2$ (\mathbb{R}^3) are the position and velocity of i th robot, $\mathbf{u}_i \in \mathbb{R}^2$ (\mathbb{R}^3) is the acceleration input of the i th robot, $i = 1, 2, \dots, M$.

This system (27) could be expressed as

$$\dot{\mathbf{x}} = \mathbf{A} \mathbf{x} + \mathbf{B} \mathbf{u} \quad (28)$$

where $\mathbf{x} = [\mathbf{p}_i \ \mathbf{v}_i]^T$, $\mathbf{u} = \mathbf{u}_i$. And the discretization form is

$$\mathbf{x}_{k+1} = \mathbf{A}_k \mathbf{x}_k + \mathbf{B}_k \mathbf{u}_k \quad (29)$$

where \mathbf{x}_k and \mathbf{u}_k are state and input at the time k ,

$$\mathbf{A}_k = \begin{bmatrix} \mathbf{I} & T_s \mathbf{I} \\ \mathbf{0} & \mathbf{0} \end{bmatrix}, \mathbf{B}_k = \begin{bmatrix} \mathbf{0} \\ T_s \mathbf{I} \end{bmatrix}.$$

Dynamic Obstacles

As depicted in Fig. 8(a), for a robot i in the swarm, regard other robot j as the dynamic obstacle which is represented by an ellipse of area $\mathcal{O}_{j,k}$ at time k . The ellipse of area $\mathcal{O}_{j,k}$ at time k is denoted by

$$\mathcal{O}_{j,k} = \{\mathbf{p} \mid \|\mathbf{E}(\mathbf{p} - \mathbf{p}_{j,k})\| \leq 1\}, k = 0, 1, \dots, N, \quad (30)$$

where $\mathbf{p}_{j,k}$ is the position of the center mass of the robot j at time k , $\mathbf{E} = \text{diag}(a_j, b_j, c_j)$ is an invertible scaling matrix to bound the boundary of ellipse. The details of designing \mathbf{E} are in Quan et al. (2023a). If the robot i is regarded as a mass point, the obstacle space \mathcal{O}_k of robot i at time k is expressed as

$$\mathcal{O}_k = \bigcup_{j \in \mathcal{M}, j \neq i} \mathcal{O}_{j,k}, \quad (31)$$

where $\mathcal{O}_{i,j,k} = \{\mathbf{p} \mid \mathbf{p} \in \mathcal{O}_{i,k} \oplus \mathcal{O}_{j,k}\}$, \oplus is the Minkowski sum. However, when the robot i does not collide with other robots, the avoidance constraints

$$\mathbf{p}_{i,k} \cap \mathcal{O}_k = \emptyset \quad (32)$$

are not convex constraints. Thus, half spaces $\mathcal{H}_{ij,k}$, as shown in Fig. 8(b), are used to construct affine inequality constraints at each time k . The constrains (32) are transformed into

$$\mathcal{O} = \{\mathbf{x}_k \mid \mathbf{H}_k \mathbf{x}_k \leq h_k + s_k, k = 0, 1, \dots, N\}, \quad (33)$$

where \mathbf{x}_k are states of robot i , \mathbf{H}_k , h_k are parameters of half space constraints, s_k is a positive relaxation variable to avoid infeasibility problem in practice.

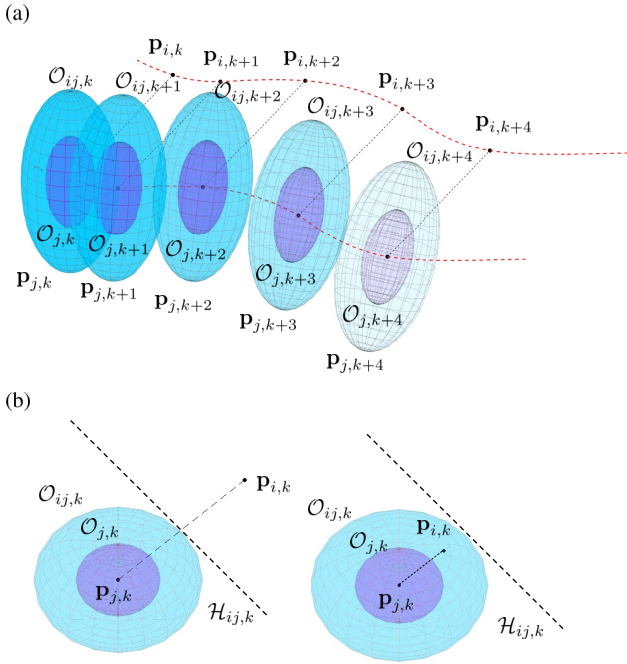


Figure 8. Constructing constraints for avoiding collisions. The purple ellipses $\mathcal{O}_{j,k+n}$ ($n = 0, 1, \dots, 4$) are boundaries of robot j at time $k + n$. The blue ellipses $\mathcal{O}_{i,k+n}$ ($n = 0, 1, \dots, 4$) are obstacle space for robot i at time $k + n$. (a) The obstacle constraints for robot i at time $k + n$. (b) Two situations: collision and avoidance. The dotted lines are tangent planes $\mathcal{H}_{ij,k}$ of points which are intersections of surfaces of blue ellipses and connections of points $\mathbf{p}_{j,k}, \mathbf{p}_{i,k}$.

Optimization Problem

The distance to desired state $\mathbf{x}_{d,k} = [\mathbf{p}_{d,k} \quad \mathbf{v}_{d,k}]^T$ and desired input $\mathbf{u}_{d,k}$ at time k generated by desired trajectory $\mathbf{h}^*((\mathbf{q}_0, \mathbf{q}_m), t(s))^\dagger$ is minimized so that the robot could track the desired trajectory. Thus, the optimization problem is concluded as

$$\begin{aligned} \min \quad & \tilde{\mathbf{x}}_N^T \mathbf{Q}_{x,N} \tilde{\mathbf{x}}_N + \sum_{k=0}^N q_{s,k} s_k^2 + \sum_{k=0}^{N-1} \tilde{\mathbf{x}}_k^T \mathbf{Q}_{x,k} \tilde{\mathbf{x}}_k + \\ & \tilde{\mathbf{u}}_k^T \mathbf{Q}_{u,k} \tilde{\mathbf{u}}_k \\ \text{s.t.} \quad & \mathbf{x}_{k+1} = \mathbf{A}_k \mathbf{x}_k + \mathbf{B}_k \mathbf{u}_k \\ & \mathbf{x}_k \in \mathcal{X} \cap \mathcal{O}, \\ & \mathbf{u}_k \in \mathcal{U}, \\ & k = 0, 1, \dots, N, \end{aligned} \quad (34)$$

where $\tilde{\mathbf{x}}_k = \mathbf{x}_{d,k} - \mathbf{x}_k$, $\tilde{\mathbf{u}}_k = \mathbf{u}_{d,k} - \mathbf{u}_k$, $\mathbf{Q}_{x,k}$ and $\mathbf{Q}_{u,k}$ are positive definite coefficient matrixs, \mathcal{X} is the feasible set of \mathbf{x}_k , \mathcal{U} is the feasible set of \mathbf{u}_k .

Simulation and Experiments

This section presents simulations and experiments of drone swarm to validate and demonstrate the effectiveness of the proposed optimal virtual tube planning method and the MPC controller.

Simulations

The results of the optimal virtual tube planning and trajectories tracking are obtained. To demonstrate the

effectiveness of the proposed method, the comparison between the optimal virtual tube planning and a traditional planning method are made in 2-D and 3-D space. The simulation results demonstrate that the proposed method with a computational complexity $O(1)$ produces the same results as the traditional planning method with a computational complexity $O(n^2)$, while requiring less computational effort. The optimal virtual tube planning and trajectories tracking are implemented using MATLAB code, and executed on a PC with Intel Core i7-7700 @ 2.8GHz CPU and 16G RAM. The safety distance between drones is 1m.

A 2-D optimal virtual tube The optimal virtual tube planning is first validated in a 2-D map. Two methods were set with identical terminals \mathcal{C}_0 and \mathcal{C}_1 , as illustrated in Fig. 9 with dotted lines. Additionally, 11 start positions and 11 goal positions are also the same. For the traditional planning method, 11 separate optimization problems are required to be solved, as depicted in Fig. 9(a). In contrast, for the proposed method, only two trajectories need to be planned: black lines in Fig. 9(b). The remaining 9 trajectories, depicted by red lines in Fig. 9(b), are generated by interpolation of two planned trajectories. Similarly, 101 trajectories are generated in the same way, requiring the resolution of only two optimization problems for two trajectories. Comparing the optimal variable vector of traditional method with those generated through interpolation, the errors were found to be negligible, with magnitudes less than 1.8×10^{-14} m, as shown in Fig. 10. Thus, this outcome validates *Theorem 1*. To demonstrated that the error is independent of the number of interpolation, a randomly selected parameter in variable vector is analyzed and its distribution is shown with respect to number of trajectories obtained by interpolation in Fig. 11. The results show that the error for this parameter remain stable as the number of interpolation increasing from 10 to 1000.

In Fig. 9(b), the terminal \mathcal{C}_0 is represented by a line with a length of $10m$. To validate the controller, 11 drones are tightly placed in the terminal \mathcal{C}_0 , as shown in Fig. 12. Then, 11 optimal trajectories are assigned to each drone. In the result of simulation depicted in Fig. 12, the drone swarm safely and smoothly arrives at terminal \mathcal{C}_1 . When the drones are far apart, they follows their own trajectories. However, when the swarm passes through a narrow cross-section of virtual tube in Fig. 12, some drones need to avoid nearby drones, which may cause them to deviate from their trajectories ($t = 12.96$ s) but return to them after passing through the narrow space ($t = 14.80$ s). The minimum distance between drones in swarm with respect to time shown in Fig. 13 is always greater than the safety distance $1m$, which depicts that there is no collision among drones. To demonstrate the accuracy of drone tracking, errors between desired and true trajectory of all drones are depicted in Fig. 14. Therefore, the simulation demonstrates that every

[†]In practice, the normalized knots $\{t_i\}$ are not suitable for a robot to track trajectory. To address this issue, the $t(s) = \frac{v_R}{u_m} s$ is used in the trajectory $\mathbf{h}^*((\mathbf{q}_0, \mathbf{q}_m), t(s))$, where v_R is a coefficient related with robots, $u_m \in \{u_i\}$.

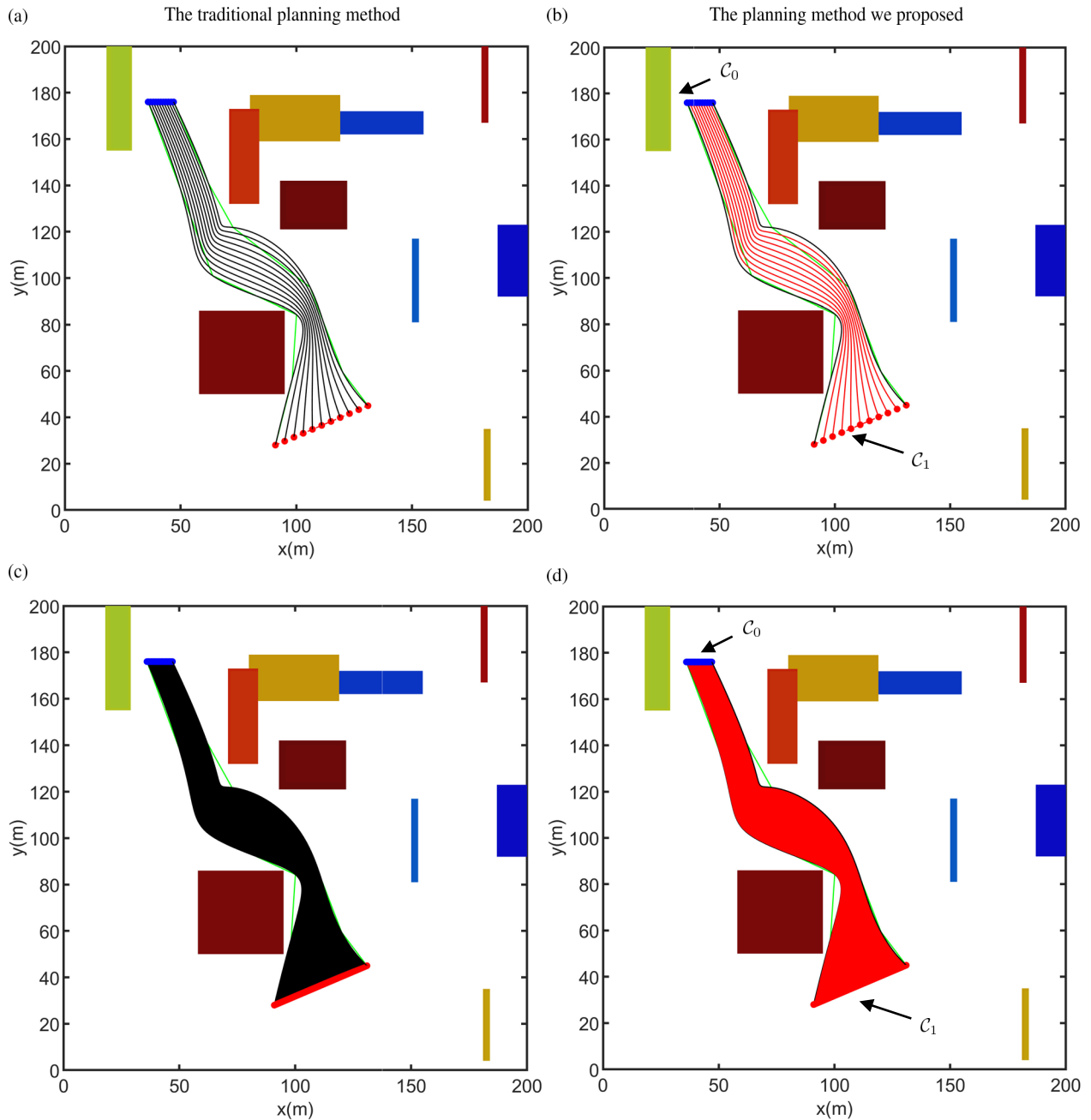


Figure 9. Comparison between the traditional method and the optimal virtual tube planning. (a) Trajectories planned by 11 different optimization problems with the traditional method. (b) Trajectories planned only by two optimization problems with the optimal virtual tube planning. (c) Trajectories planned by 101 different optimization problems with the traditional method. (d) Trajectories planned only by two optimization problems with the optimal virtual tube planning. The colorful rectangles are obstacles. The blue points and the red points are start points and goal points. The optimal trajectories planned by optimization problems are depicted in black, while the optimal trajectories obtained by interpolation are shown in red. The magenta dotted lines denote the terminals.

drone can track the trajectory with high accuracy while avoiding other drones.

A 3-D optimal virtual tube For a $240\text{m} \times 240\text{m} \times 120\text{m}$ map, illustrated in Fig. 15(a), the start terminal C_0 which is the convex hull of the set $\{\mathbf{q}_{0,k}\}$ is represented as a green tetrahedroid, while the goal terminal C_1 which is the convex hull of the set $\{\mathbf{q}_{m,k}\}$ is represented as a red tetrahedroid. First, the order pairs $(\mathbf{q}_{0,k}, \mathbf{q}_{m,k})$ are constructed by assigning the red points to green points respectively. Thus, any start point $\mathbf{q}_0(\theta_j)$ in terminal C_0 is expressed as (11), and the map \mathbf{f} maps this point to

the goal point $\mathbf{q}_m(\theta_j)$. Then, a set of order pairs \mathcal{P} is constructed as $\{(\mathbf{q}_0(\theta_j), \mathbf{q}_m(\theta_j))\}$. Next, the paths of the order pairs $(\mathbf{q}_{0,k}, \mathbf{q}_{m,k})$ are generated by a tree-based motion planner called RRT*, as shown in Fig. 15(b). The optimal trajectories \mathbf{h}^* of the order pairs $(\mathbf{q}_{0,k}, \mathbf{q}_{m,k})$ are then obtained by solving optimization problems, as depicted in Fig. 15(c). Finally, the optimal virtual tube is generated based on Theorem 1, which is illustrated in Fig. 15(d).

The drone swarm comprises 84 drones, and their start and goal points are generated by equispaced interpolation. Subsequently, the 84 optimal trajectories for all drones are generated by interpolation between four optimal trajectories.

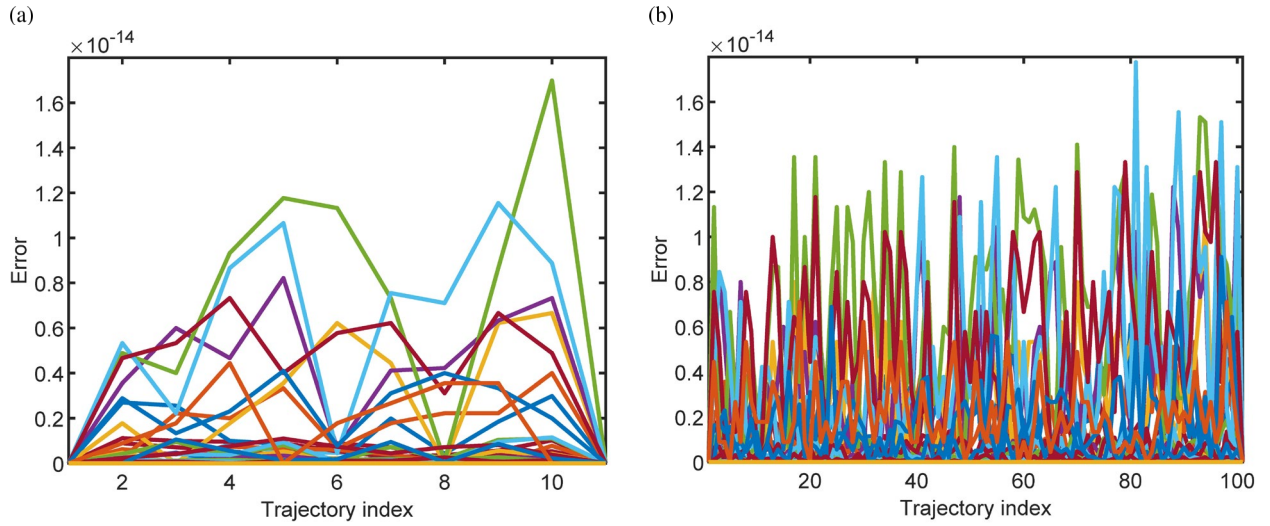


Figure 10. The errors between variable vectors by interpolation and optimization program are illustrated using colorful lines representing the error in each parameter of the variable vectors. (a) The errors of 11 trajectories. (b) The errors of 101 trajectories.

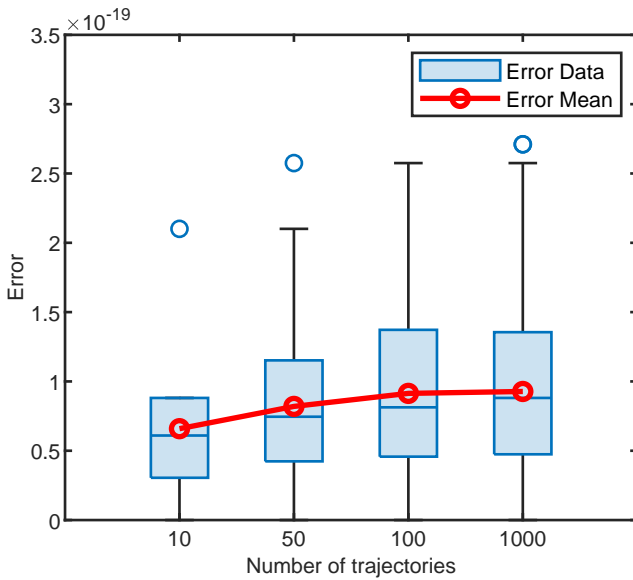


Figure 11. The error of a parameter in variable vector.

The error between the trajectories by interpolation and by solving 84 optimization problems, as shown in Fig. 16, is negligible. Then, drones could track their respective trajectories.

The terminals \mathcal{C}_0 and \mathcal{C}_1 in Fig. 15(a) are tetrahedroids. The drone swarm with 84 drones is placed in the terminal \mathcal{C}_0 . There are only 4 trajectories being planned and other 80 trajectories being generated by interpolation. In the simulation result shown in Fig. 17, the drone swarm arrives in terminal \mathcal{C}_1 safely and smoothly. The minimum distance among drones in swarm with respect to time shown in Fig. 18 is always higher than safety distance, which demonstrates that there is no collision among drone swarm.

Experiments

A 30m×10m×8m space for real flight is depicted in Fig. 20. Known obstacles are randomly positioned on the ground within this area, and a VICON motion capture system is

utilized for drone localization. The drone depicted in Fig. 21, which has a wheelbase of 350 millimeters, is equipped with a Jetson NX for onboard computation and utilizes the CUAUV5 nano Autopilot as its flight controller.

Task Settings The designated flight area is partitioned into three distinct regions, namely the starting area, obstacle area, and goal area. The primary objective of this task for a swarm of four drones is to initiate their flight from the starting area, navigate through the obstacle area without any collision, and ultimately reach the goal area.

Optimal Virtual Tube Planning Firstly, the initial positions $\mathbf{q}_{0,k}$ of four drones in start area must be specified, as depicted in Fig. 22. The Drone 1, Drone 2, and Drone 3 are assigned to $\mathbf{q}_{0,1}$, $\mathbf{q}_{0,2}$, $\mathbf{q}_{0,3}$ respectively whose convex hull is the terminal \mathcal{C}_0 in the start area. And the position $\mathbf{q}_{0,4}$ of Drone 4 is the affine combination of $\{\mathbf{q}_{0,k}\}$ within the terminal \mathcal{C}_0 , which is expressed as

$$\mathbf{q}_{0,4} = \theta_{1,4}\mathbf{q}_{0,1} + \theta_{2,4}\mathbf{q}_{0,2} + \theta_{3,4}\mathbf{q}_{0,3}, \sum_{k=1}^3 \theta_{k,4} = 1. \quad (35)$$

Similarly, the goal positions $\mathbf{q}_{m,k}$ of drones are assigned. Specially, the goal position $\mathbf{q}_{m,4}$ is expressed as

$$\mathbf{q}_{m,4} = \theta_{1,4}\mathbf{q}_{m,1} + \theta_{2,4}\mathbf{q}_{m,2} + \theta_{3,4}\mathbf{q}_{m,3}, \sum_{k=1}^3 \theta_{k,4} = 1. \quad (36)$$

Thus, the order pairs $(\mathbf{q}_{0,k}, \mathbf{q}_{m,k})$ are obtained.

Subsequently, path finding is used to generate paths for the three drones, as depicted in Fig. 23(a). For each order pair $(\mathbf{q}_{0,k}, \mathbf{q}_{m,k})$ ($k = 1, 2, 3$), there are 8 intermediate configurations, with $m = 7$ denoting the final configuration. To parameterize the trajectories, normalized knots t_i are automatically generated. Three optimization problems are then solved to obtain the optimal trajectories shown in Fig. 23(b), which are formulated as following:

$$\begin{aligned} \mathbf{h}^*((\mathbf{q}_{0,1}, \mathbf{q}_{7,1}), t) &= \mathbf{C}(t) \mathbf{x}_1, \\ \mathbf{h}^*((\mathbf{q}_{0,2}, \mathbf{q}_{7,2}), t) &= \mathbf{C}(t) \mathbf{x}_2, \\ \mathbf{h}^*((\mathbf{q}_{0,3}, \mathbf{q}_{7,3}), t) &= \mathbf{C}(t) \mathbf{x}_3. \end{aligned} \quad (37)$$

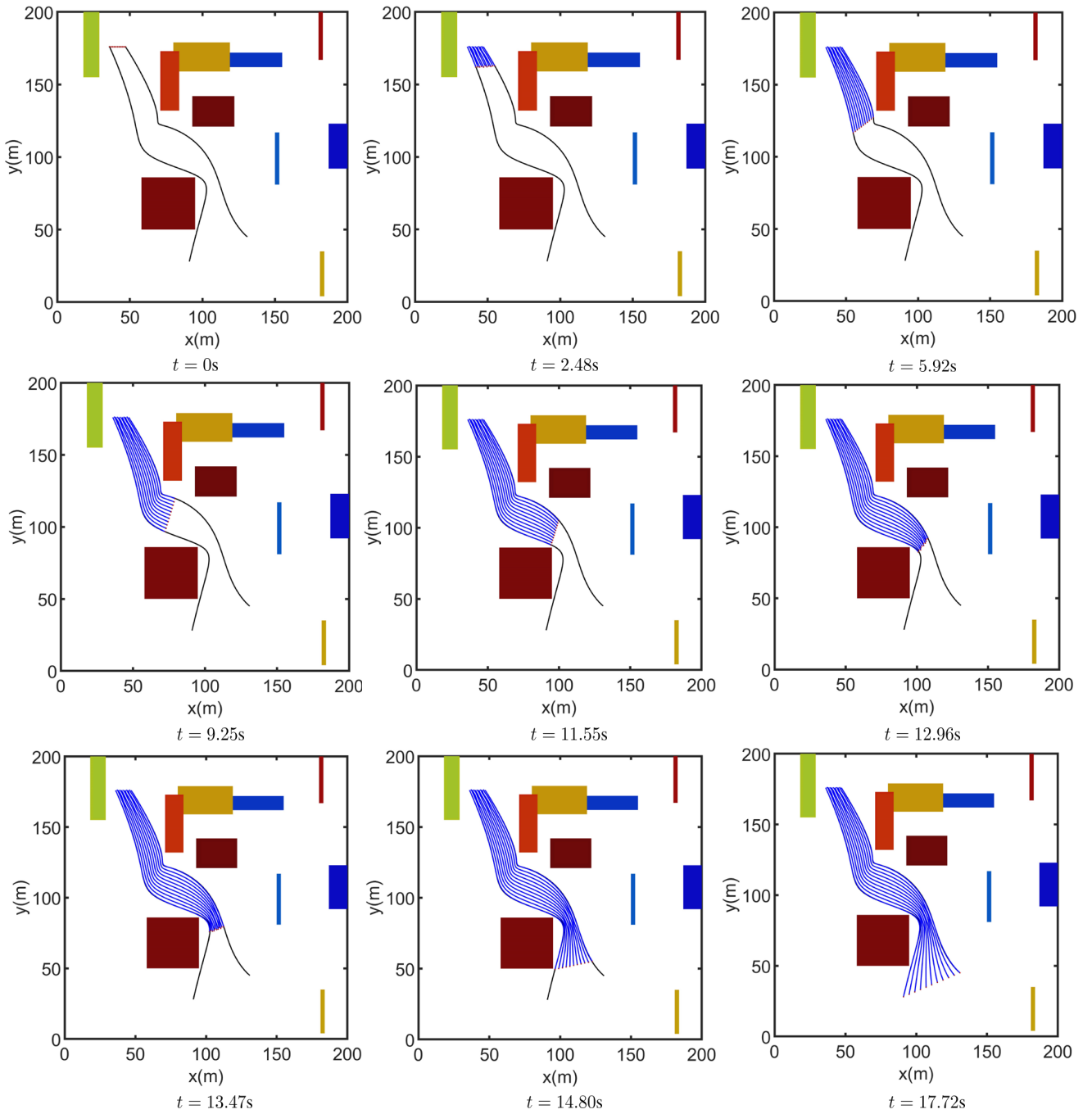


Figure 12. Simulation results of drone swarm trajectories tracking. The 11 dark blue lines are trajectories for 11 drones, while the red circles indicate drones.

Hence, utilizing *Theorem 1*, the optimal virtual tube $(\mathcal{C}_0, \mathcal{C}_1, \mathbf{f}, \mathbf{h}^*)$ is constructed. Since the position $\mathbf{q}_{0,4}$ is located in the terminal \mathcal{C}_0 , the optimal trajectory $\mathbf{h}^*((\mathbf{q}_{0,4}, \mathbf{q}_{7,4}), t)$ for drone 4 can be generated by

$$\mathbf{h}^*((\mathbf{q}_{0,4}, \mathbf{q}_{7,4}), t) = \mathbf{C}(t) \sum_{k=1}^3 \theta_{k,4} \mathbf{x}_k, \quad (38)$$

as illustrated in Fig. 23(c). Upon obtaining the four trajectories for the drones, each drone can track its own trajectory while avoiding the others, as depicted in Fig. 23(d).

Discussion

The planning of optimal virtual tubes in 2-D and 3-D space are simulated to verify the correctness of *Theorem 1*. And the MPC controller is implemented to achieve inter-drone collision avoidance while tracking the trajectory. Simulation results demonstrate that the proposed method of optimal virtual tube planning is applicable to large-scale swarm movements. The number of optimization problems is independent of the number of drones, when start positions of drones are within the terminal \mathcal{C}_0 .

In the real flight depicted in Fig. 24, the 4th optimal trajectory of Drone 4, is generated by the affine combination of three optimal trajectories which construct the optimal

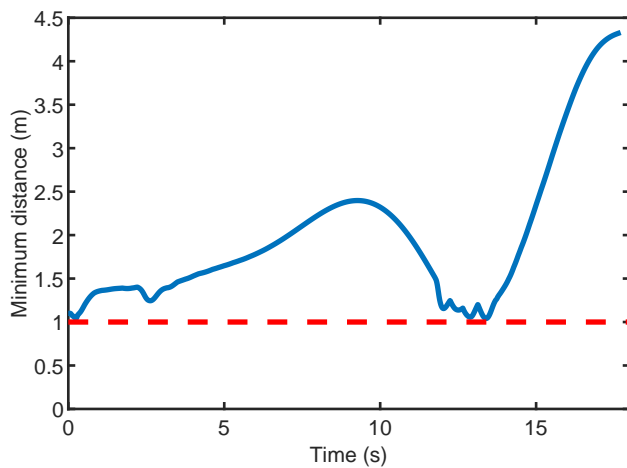


Figure 13. The minimum distance among drones. The blue line is the minimum distance with respect to time. The red dotted line is the safety distance among drones.

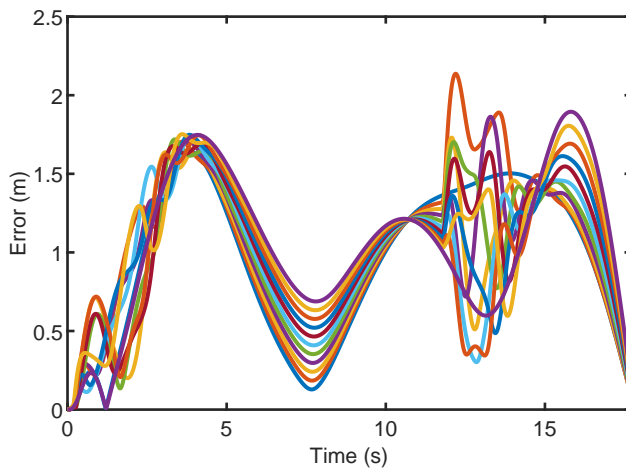


Figure 14. Comparison of actual and desired trajectories for the drone swarm.

virtual tube. Subsequently, drone swarm successfully track their respective trajectories to pass through environment. The velocity of randomly selected Drone 2 with respect to time is shown in Fig. 25, which indicates that drone swarm can fast and smoothly pass through the optimal virtual tube. However, the current path finding method may not be suitable for virtual tube planning, as the paths found may not be homotopic due to the presence of obstacles between them.

Furthermore, the optimal virtual tube could be used for a single drone. if the start terminal C_0 shrinks into a point, the drone in the start terminal C_0 would be assigned with infinite optimal trajectories whose goal points are in the terminal C_1 .

Conclusion and Future Work

This paper extends definition of the virtual tube, proposes optimal virtual tubes, and analyzes their properties. One type of virtual tube, namely the linear virtual tube with convex hull terminals, is used for constructing optimal virtual tube. Then, a planning method of this linear virtual tube with convex hull terminals is proposed and its effectiveness is

demonstrated in simulations. The results in 2-D and 3-D show that the error between interpolation and optimization is negligible. Therefore, our method can efficiently reduce the computation and generate infinite optimal trajectories. An application of the optimal virtual tube, which uses an MPC controller for drone swarm to track the trajectories, shows that it can be used in real flight. In future work, a suitable path finding algorithm for the virtual tube will be designed and the network of the virtual tube will be explored.

References

- Alonso-Mora J, Baker S and Rus D (2017) Multi-robot Formation Control and Object Transport in Dynamic Environments via Constrained Optimization. *The International Journal of Robotics Research* 36(9): 1000–1021.
- Boyd SP and Vandenberghe L (2004) *Convex Optimization*. Cambridge University Press.
- Deits R and Tedrake R (2015) Efficient Mixed-integer Planning for UAVs in Cluttered Environments. In: *2015 IEEE International Conference on Robotics and Automation (ICRA)*. IEEE, pp. 42–49.
- Ding W, Gao W, Wang K and Shen S (2019) An Efficient B-Spline-Based Kinodynamic Replanning Framework for Quadrotors. *IEEE Transactions on Robotics* 35: 1287–1306.
- Gao F, Wang L, Zhou B, Zhou X, Pan J and Shen S (2020) Teach-Repeat-Replan: A Complete and Robust System for Aggressive Flight in Complex Environments. *IEEE Transactions on Robotics* 36(5): 1526–1545.
- Gao Y, Bai C and Quan Q (2022) Distributed Control for a Multi-Agent System to Pass through a Connected Quadrangle Virtual Tube. *IEEE Transactions on Control of Network Systems* : 1–12.
- Karaman S and Frazzoli E (2011) Sampling-based Algorithms for Optimal Motion Planning. *The International Journal of Robotics Research* 30(7): 846–894.
- Liu S, Watterson M, Mohta K, Sun K, Bhattacharya S, Taylor CJ and Kumar V (2017) Planning Dynamically Feasible Trajectories for Quadrotors Using Safe Flight Corridors in 3-D Complex Environments. *IEEE Robotics and Automation Letters* 2: 1688–1695.
- Mao P and Quan Q (2022) Making Robotics Swarm Flow More Smoothly: A Regular Virtual Tube. In: *IEEE/RSJ International Conference on Intelligent Robots and Systems (IROS)*. pp. 4498–4504.
- Mellinger D and Kumar V (2011) Minimum Snap Trajectory Generation and Control for Quadrotors. In: *2011 IEEE International Conference on Robotics and Automation*. IEEE, pp. 2520–2525.
- Orthey A, Frész B and Toussaint M (2019) Motion Planning Explorer: Visualizing Local Minima Using A Local-minima Tree. *IEEE Robotics and Automation Letters* 5(2): 346–353.
- Osa T (2022) Motion Planning by Learning the Solution Manifold in Trajectory Optimization. *The International Journal of Robotics Research* 41(3): 281–311.
- Park J and Kim HJ (2021) Online Trajectory Planning for Multiple Quadrotors in Dynamic Environments Using Relative Safe Flight Corridor. *IEEE Robotics and Automation Letters* 6: 659–666.

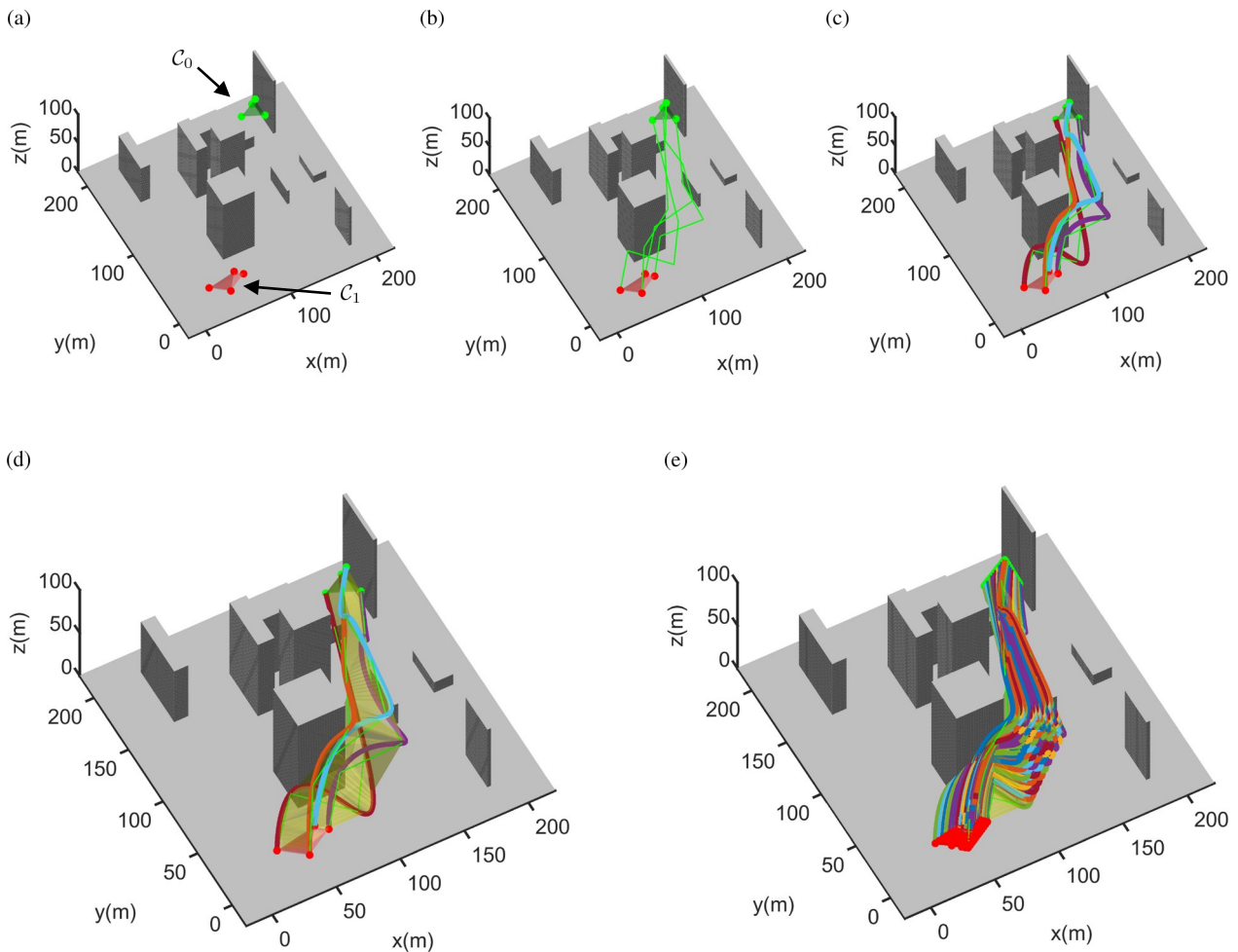


Figure 15. The optimal virtual tube planning process. (a) Constructing order pairs \mathcal{P} . The red points represent the start points, and the green points represent the goal points. The red trigonal pyramid denotes the start area, and the green trigonal pyramid denotes the goal area. (b) Finding paths. A path-finding algorithm is used to find paths, shown as green lines. (c) Optimizing trajectories. Optimal trajectories are generated by solving optimization problems. The colorful lines represent different trajectories for different pairs. (d) Constructing optimal virtual tube. An optimal virtual tube is generated based on the optimal trajectories, shown as a yellow area. (e) Containing infinite optimal paths. Other optimal trajectories, denoted by colorful lines, are automatically generated by interpolation.

- Piegl LA and Tiller W (2000) Surface Approximation to Scanned Data. *The Visual Computer* 16(7): 386–395.
- Quan Q, Fu R and Cai KY (2023a) How Far Two UAVs Should be Subject to Communication Uncertainties. *IEEE Transactions on Intelligent Transportation Systems* 24(1): 429–445.
- Quan Q, Fu R, Li M, Wei D, Gao Y and Cai KY (2022) Practical Distributed Control for VTOL UAVs to Pass a Virtual Tube. *IEEE Transactions on Intelligent Vehicles* 7(2): 342–353.
- Quan Q, Yan G and Chenggang B (2023b) Distributed Control for a Robotic Swarm to Pass Through a Curve Virtual Tube. *Robotics and Autonomous Systems* 162: 104368.
- Richter C, Bry A and Roy N (2016) Polynomial trajectory planning for aggressive quadrotor flight in dense indoor environments. In: *Robotics Research: The 16th International Symposium ISRR*. pp. 649–666.
- Shick PL (2007) *Topology: Point-set and Geometric*. Wiley-Interscience.
- Soria E, Schiano F and Floreano D (2022) Distributed Predictive Drone Swarms in Cluttered Environments. *IEEE Robotics and Automation Letters* 7(1): 73–80.
- Strothotte T and Schlechtweg S (2002) 7 - Geometric Models and Their Exploitation in NPR. In: *Non-Photorealistic Computer Graphics*, The Morgan Kaufmann Series in Computer Graphics. Morgan Kaufmann, pp. 203–245.
- Tang S, Thomas J and Kumar V (2018) Hold or take optimal plan (hoop): A Quadratic Programming Approach to Multi-robot Trajectory Generation. *The International Journal of Robotics Research* 37(9): 1062–1084.
- Tu LW (2011) *An Introduction to Manifolds*. Springer.
- Usenko V, von Stumberg L, Pangercic A and Cremers D (2017) Real-time Trajectory Replanning for MAVs using Uniform B-splines and A 3D Circular Buffer. In: *2017 IEEE/RSJ International Conference on Intelligent Robots and Systems (IROS)*. IEEE, pp. 215–222.
- Zhou B, Gao F, Pan J and Shen S (2020) Robust Real-time UAV Replanning Using Guided Gradient-based Optimization and Topological Paths. In: *2020 IEEE International Conference on Robotics and Automation (ICRA)*. IEEE, pp. 1208–1214.
- Zhou B, Gao F, Wang L, Liu C and Shen S (2019) Robust and Efficient Quadrotor Trajectory Generation for Fast

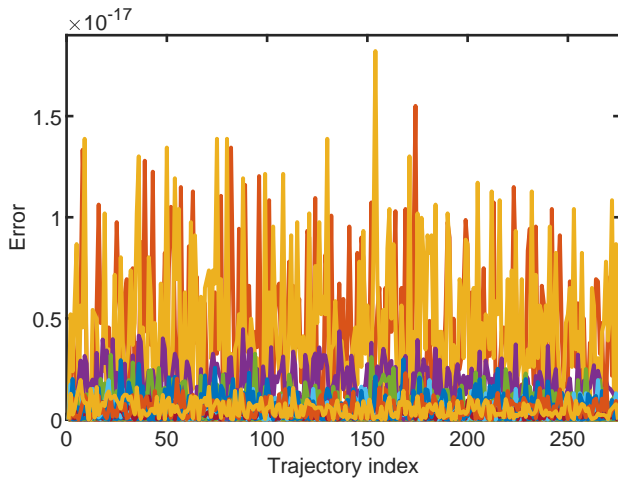


Figure 16. The errors between variable vectors of trajectories by interpolation and optimization problem are illustrated using colorful lines representing the error in each parameter of the variable vectors.

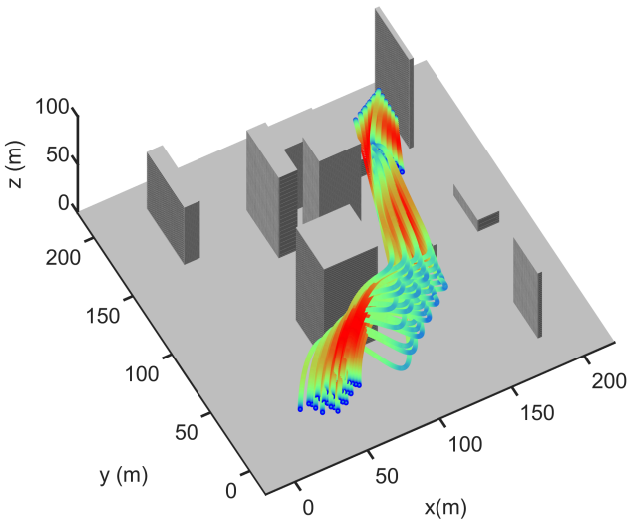


Figure 17. Simulation results of drone swarm following in 3-D. The colorful lines are different trajectories.

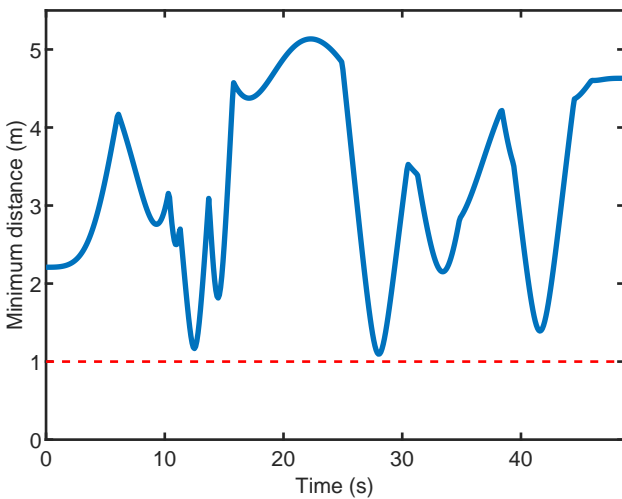


Figure 18. The minimum distance among drones in 3-D. The red dotted line is 1m line.

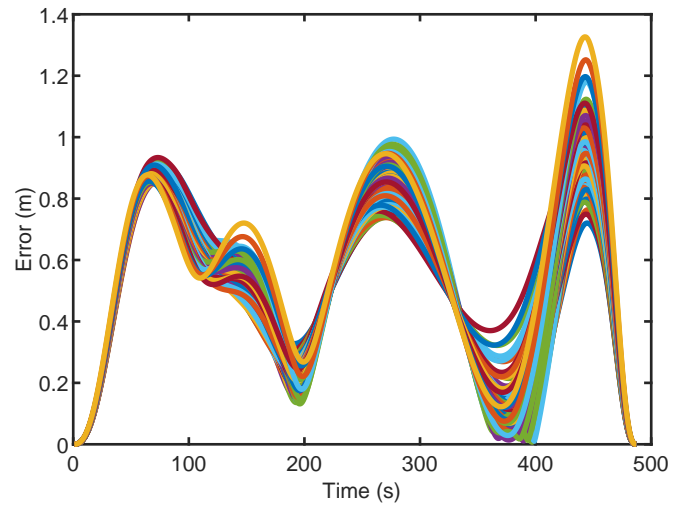


Figure 19. The comparison between desired and actual trajectory for the drone swarm.



Figure 20. The space for real flight.



Figure 21. The drone used for real flight.

Autonomous Flight. *IEEE Robotics and Automation Letters* 4(4): 3529–3536.

Zhou X, Wang Z, Ye H, Xu C and Gao F (2021a) EGO-Planner: An ESDF-Free Gradient-Based Local Planner for Quadrotors. *IEEE Robotics and Automation Letters* 6(2): 478–485.

Zhou X, Zhu J, Zhou H, Xu C and Gao F (2021b) EGO-Swarm: A Fully Autonomous and Decentralized Quadrotor Swarm System in Cluttered Environments. In: *2021 IEEE International Conference on Robotics and Automation (ICRA)*. IEEE, pp. 4101–4107.

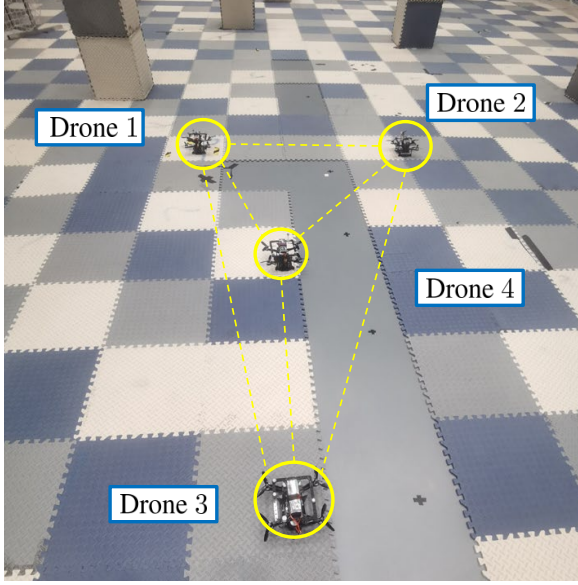


Figure 22. The positions of drones in the start area.

A The Proofs of Lemma 1 and Lemma 2

A.1 Proof of Lemma 1

Proof. In *Step 1*, it is proved that $\mathbf{x}(\boldsymbol{\theta})$ is feasible. Then $\mathbf{x}(\boldsymbol{\theta})$ being optimal is shown in *Step 2*.

Step 1. According to an optimality criterion (Boyd and Vandenberghe (2004)) for differentiable f_0 . Let \mathcal{X}_θ , \mathcal{X}_k denote the feasible set:

$$\mathcal{X}_\theta = \{\mathbf{x} | \mathbf{A}\mathbf{x} = \mathbf{b}(\boldsymbol{\theta})\}, \mathcal{X}_k = \{\mathbf{x} | \mathbf{A}\mathbf{x} = \mathbf{b}_k\}.$$

Then for all $\mathbf{x} \in \mathcal{X}_k$,

$$\nabla f_0(\mathbf{x}_k)^\top (\mathbf{x} - \mathbf{x}_k) \geq 0, k = 1, 2, \dots, q. \quad (39)$$

Since \mathbf{x}_k is feasible, each solution \mathbf{x} in Equation (39) can be expressed as the combination of a special solution and a solution in zero space, such as $\mathbf{x} = \mathbf{x}_k + \mathbf{v}, \mathbf{v} \in N(\mathbf{A})$. Therefore, this optimal condition (39) can be transformed into

$$\nabla f_0(\mathbf{x}_k)^\top \mathbf{v} \geq 0, \text{ for all } \mathbf{v} \in N(\mathbf{A}). \quad (40)$$

When $\mathbf{b} = \mathbf{b}(\boldsymbol{\theta})$, substitute $\mathbf{x}(\boldsymbol{\theta})$ into (6) to obtain

$$\mathbf{A}\mathbf{x}(\boldsymbol{\theta}) = \sum_{k=0}^q \theta_k \mathbf{A}\mathbf{x}_k = \sum_{k=0}^q \theta_k \mathbf{b}_k = \mathbf{b}(\boldsymbol{\theta}).$$

Therefore, $\mathbf{x}(\boldsymbol{\theta})$ is feasible.

Step 2. For all $\mathbf{x} \in \mathcal{X}_\theta$, it has

$$\nabla f_0(\mathbf{x}(\boldsymbol{\theta}))^\top (\mathbf{x} - \mathbf{x}(\boldsymbol{\theta})) = \sum_{k=0}^q \theta_k \nabla f_0(\mathbf{x}_k)^\top \mathbf{v}. \quad (41)$$

Combine Equation (41) with (40), it is derived that

$$\nabla f_0(\mathbf{x}(\boldsymbol{\theta}))^\top (\mathbf{x} - \mathbf{x}(\boldsymbol{\theta})) \geq 0, \text{ for all } \mathbf{x} \in \mathcal{X}_\theta. \quad (42)$$

Therefore, $\mathbf{x}(\boldsymbol{\theta})$ is optimal.

A.2 Proof of Lemma 2

Proof. In *Step 1*, it is shown that $\mathbf{x}(\boldsymbol{\theta})$ is feasible. Then $\mathbf{x}(\boldsymbol{\theta})$ being optimal is shown in *Step 2*.

Step 1. According to an optimality criterion (Boyd and Vandenberghe (2004)) for differentiable f_0 . Let \mathcal{X}_θ , \mathcal{X}_k denote the feasible set,

$$\mathcal{X}_\theta = \{\mathbf{x} | \mathbf{A}\mathbf{x} = \mathbf{b}(\boldsymbol{\theta}), f_i(\mathbf{x}) \leq 0, i = 1, \dots, n_c\},$$

$$\mathcal{X}_k = \{\mathbf{x} | \mathbf{A}\mathbf{x} = \mathbf{b}_k, f_i(\mathbf{x}) \leq 0, i = 1, \dots, n_c\}.$$

Let \mathcal{V}_k denote the equivalent feasible set,

$$\mathcal{V}_k = \{\mathbf{v} | \mathbf{A}(\mathbf{x}_k + \mathbf{v}) = \mathbf{b}_k, f_i(\mathbf{x}_k + \mathbf{v}) \leq 0, i = 1, \dots, n_c\}.$$

And for all $\mathbf{x} \in \mathcal{X}_k$,

$$\nabla f_0(\mathbf{x}_k)^\top (\mathbf{x} - \mathbf{x}_k) \geq 0. \quad (43)$$

Since \mathbf{x}_k is feasible, every \mathbf{x} has $\mathbf{x} = \mathbf{x}_k + \mathbf{v}$, $\mathbf{v} \in \mathcal{V}_k$. Therefore, the optimal condition (43) can be expressed as:

$$\nabla f_0(\mathbf{x}_k)^\top \mathbf{v} \geq 0, \text{ for all } \mathbf{v} \in \mathcal{V}_k. \quad (44)$$

Let \mathbf{b} be $\mathbf{b}(\boldsymbol{\theta})$, substitute $\mathbf{x}(\boldsymbol{\theta})$ into constraints to obtain

$$\mathbf{A}\mathbf{x}(\boldsymbol{\theta}) = \sum_{k=0}^q \theta_k \mathbf{A}\mathbf{x}_k = \sum_{k=0}^q \theta_k \mathbf{b}_k = \mathbf{b}(\boldsymbol{\theta}),$$

$$f_j(\mathbf{x}(\boldsymbol{\theta})) \leq \sum_{k=0}^q \theta_k f_j(\mathbf{x}_k) \leq 0, j = 1, \dots, n_c.$$

Therefore, $\mathbf{x}(\boldsymbol{\theta})$ is feasible.

Then, for all $\mathbf{x} \in \mathcal{X}_\theta$, it has equivalent constraint $\mathcal{V}_\theta = \sum_{k=0}^q \theta_k \mathcal{V}_k$. Therefore, for all $\mathbf{v}_\theta \in \mathcal{V}_\theta$, there exist $\mathbf{v}_k \in \mathcal{V}_k$ so that

$$\mathbf{v}_\theta = \sum_{k=0}^q \theta_k \mathbf{v}_k.$$

Thus, $\mathbf{x}(\boldsymbol{\theta})$ is feasible.

Step 2. In the following, we will show $\nabla f_0(\mathbf{x}(\boldsymbol{\theta}))^\top \mathbf{v}_\theta \geq 0$.

When $q = 2$,

$$\begin{aligned} \nabla f_0(\mathbf{x}(\boldsymbol{\theta}))^\top \mathbf{v}_\theta &= (\theta_0^2 + \theta_0\theta_1) \nabla f_0(\mathbf{x}_0)^\top \mathbf{v}_0 + (\theta_1^2 + \theta_0\theta_1) \nabla f_0(\mathbf{x}_1)^\top \mathbf{v}_1 \\ &\quad + \theta_0\theta_1 (\nabla f_0(\mathbf{x}_0) - \nabla f_0(\mathbf{x}_1))^\top (\mathbf{x}_0 - \mathbf{x}_1). \end{aligned} \quad (45)$$

Since f_0 is a convex function, there have

$$f_0(\mathbf{x}_0) \geq f_0(\mathbf{x}_1) + \nabla f_0(\mathbf{x}_1)^\top (\mathbf{x}_0 - \mathbf{x}_1), \quad (46a)$$

$$f_0(\mathbf{x}_1) \geq f_0(\mathbf{x}_0) + \nabla f_0(\mathbf{x}_0)^\top (\mathbf{x}_1 - \mathbf{x}_0). \quad (46b)$$

Combine (46a) and (46b), we obtain that

$$(\nabla f_0(\mathbf{x}_0) - \nabla f_0(\mathbf{x}_1))^\top (\mathbf{x}_0 - \mathbf{x}_1) \geq 0. \quad (47)$$

Combining Equation (45) with (47), it is derived that

$$\nabla f_0(\mathbf{x}(\boldsymbol{\theta}))^\top \mathbf{v}_\theta \geq 0, \text{ for all } \mathbf{v}_\theta \in \mathcal{V}_\theta. \quad (48)$$

Suppose the Equation (48) holds when $q = n$. Then, when $q = n + 1$, we have

$$\begin{aligned} \mathbf{v}_\theta &= \theta_{n+1} \mathbf{v}_{n+1} + \sum_{k=0}^n \theta_k \mathbf{v}_k \\ &= \theta_{n+1} \mathbf{v}_{n+1} + \sum_{k=0}^n \theta_k \frac{\theta_k}{\sum_{k=0}^n \theta_k} \mathbf{v}_k \\ &= \theta_{n+1} \mathbf{v}_{n+1} + (1 - \theta_{n+1}) \sum_{k=0}^n \frac{\theta_k}{\sum_{k=0}^n \theta_k} \mathbf{v}_k, \\ \mathbf{x}_\theta &= \theta_{n+1} \mathbf{x}_{n+1} + (1 - \theta_{n+1}) \sum_{k=0}^n \frac{\theta_k}{\sum_{k=0}^n \theta_k} \mathbf{x}_k. \end{aligned} \quad (49)$$

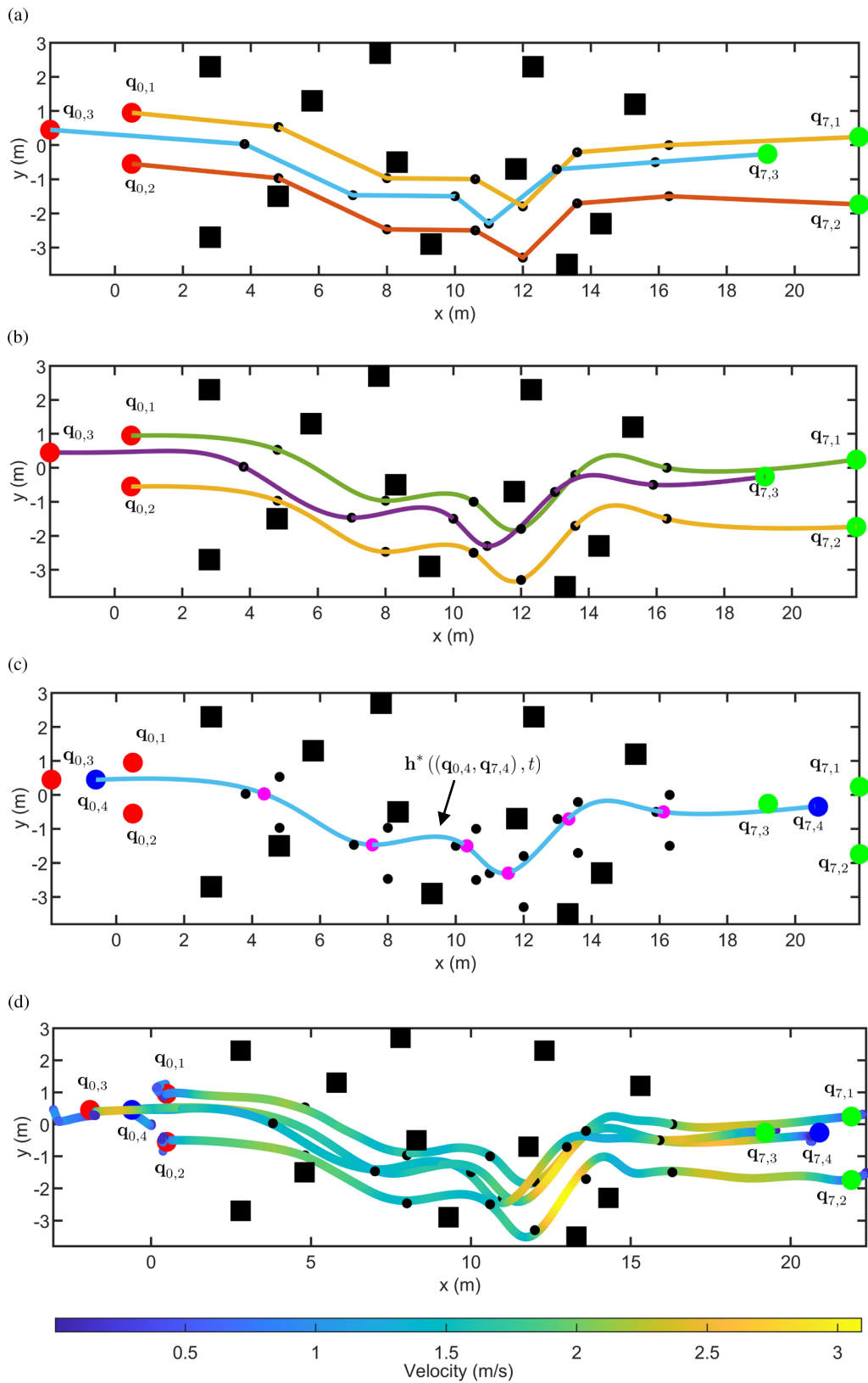


Figure 23. The process of optimal virtual tube planning and application. The squares are obstacles in reality. The red points and green points are start positions and goal positions respectively. (a) The paths for three order pairs. (b) The optimal trajectories for three order pairs. (c) The optimal trajectory of the drone 4 generated by interpolation. (d) The true trajectories of drone swarm.

We substitute (49) into (48) to obtain that $\theta_{n+1} (1 - \theta_{n+1}) \left(\nabla f_0(\mathbf{x}_{n+1}) - \nabla f_0 \left(\sum_{k=0}^n \tilde{\theta}_k \mathbf{x}_k \right) \right)^T$
 $\nabla f_0(\mathbf{x}(\boldsymbol{\theta}))^T \mathbf{v}_\theta = \theta_{n+1} \nabla f_0(\mathbf{x}_{n+1})^T \mathbf{v}_{n+1} +$
 $(1 - \theta_{n+1}) \nabla f_0 \left(\sum_{k=0}^n \tilde{\theta}_k \mathbf{x}_k \right)^T \sum_{k=0}^n \tilde{\theta}_k \mathbf{v}_k +$
 $\left(\mathbf{v}_{n+1} - \sum_{k=0}^n \tilde{\theta}_k \mathbf{v}_k \right).$

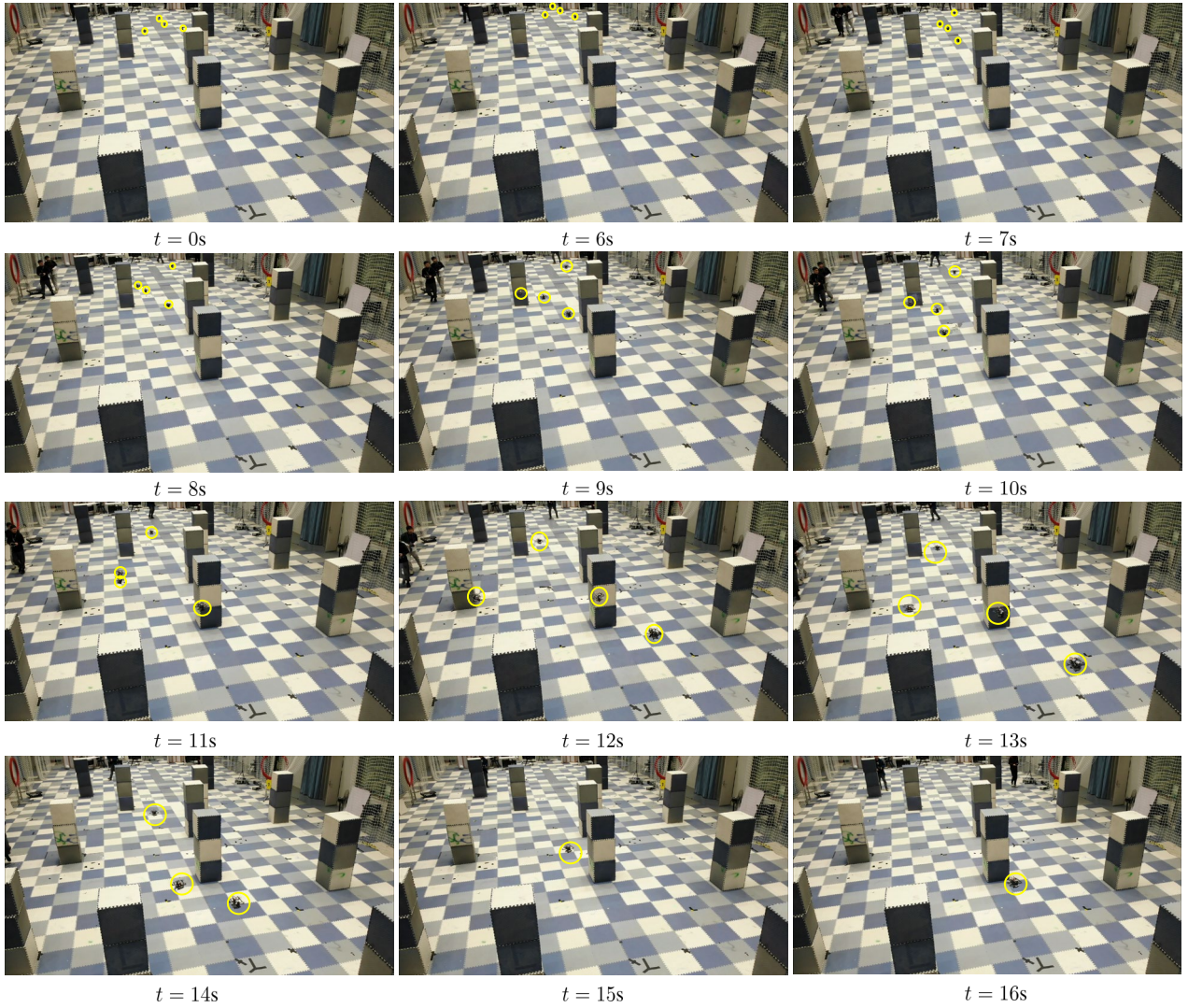


Figure 24. The real flight of drone swarm.

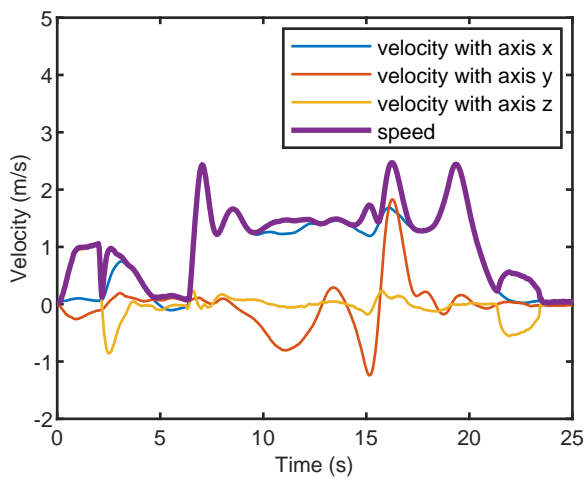


Figure 25. The velocity of Drone 2.

In the same way, we could obtain

$$\left(\nabla f_0(\mathbf{x}_{n+1}) - \nabla f_0\left(\sum_{k=0}^n \tilde{\theta}_k \mathbf{x}_k\right) \right)^T \left(\mathbf{v}_{n+1} - \sum_{k=0}^n \tilde{\theta}_k \mathbf{v}_k \right) \geq 0.$$

It is derived that

$$\nabla f_0(\mathbf{x}(\boldsymbol{\theta}))^T \mathbf{v}_\theta \geq 0, \text{ for all } \mathbf{v}_\theta \in \mathcal{V}_\theta. \quad (50)$$

Therefore, $\mathbf{x}(\boldsymbol{\theta})$ is optimal.